DISCLAIMER NOTICE

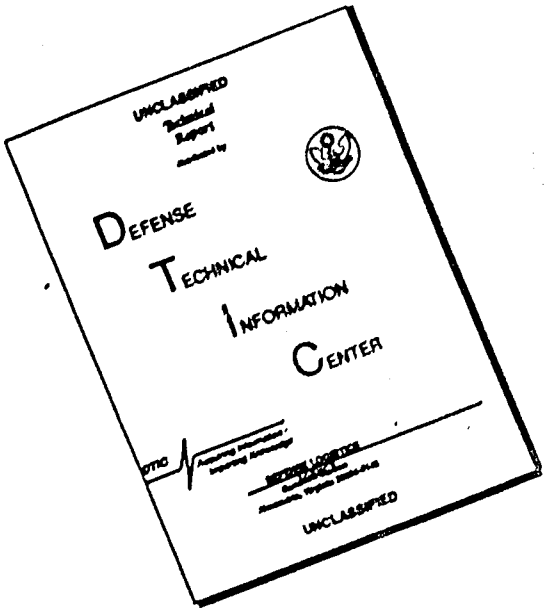

THIS DOCUMENT IS BEST QUALITY AVAILABLE. THE COPY FURNISHED TO DTIC CONTAINED A SIGNIFICANT NUMBER OF PAGES WHICH DO NOT REPRODUCE LEGIBLY.

CALCULATIONS OF THE BLAST AND CLOSE-IN ELASTIC RESPONSE OF THE CAVITY EXPLOSIONS IN THE COWBOY PROGRAM

H. L. Brode

B. R. Parkin

February 1963

P-2644

Calculations of the Blast and Close-In Elastic Response of the Cavity Explosions in the Cowboy Program

H. L. Brode and B. R. Parkin*

The RAND Corporation, Santa Monica, California

Abstract. Theoretical calculations of wall pressures and elastic wave radiations from high-explosive detonations in spherical cavities in salt are compared with close-in experimental results from the Cowboy Program. Spherical charges of Pelletol ranging from 20 to 2000 pounds (9 to 900 kg) were detonated in spherical cavities 12 and 30 feet in diameter (3.66 and 9.14 meters). The elastic wave and the wall pressure results were found to be sensitive to the explosive detonation details. New ways are suggested for correlating such quantities as explosive and radiated energies, peak values of particle displacement, velocity, acceleration, and radial stress. This correlation procedure can be useful in scaling peak particle velocities from cavity or uncoupled explosions, and is demonstrated for the Cowboy results.

*Any views expressed in this paper are those of the authors. They should not be interpreted as reflecting the views of The RAND Corporation or the official opinion or policy of any of its governmental or private research sponsors. Papers are reproduced by The RAND Corporation as a courtesy to members of its staff.

B. R. Parkin, Consultant to The RAND Corporation, now at Airesearch Manufacturing Co., Los Angeles, California.

INTRODUCTION

This paper reports the results of an investigation [Brode, 1960; Parkin, 1962] which was stimulated by the theoretical findings of A. L. Latter and his collaborators at RAND concerning the concealment of underground nuclear explosions [Latter et al., 1959; 1961]. A central idea behind this method of concealment, or "decoupling," is that if a detonation occurs in an underground cavity which is large enough to cause all displacements in the surrounding rock to stay within the "elastic" range, most of the explosive energy should leave the cavity in the form of seismic waves of high frequency which would not radiate to large distances. A very considerable fraction of the explosion energy should also remain within the hot gases contained by the cavity after the explosion. Clearly, the difficulty of detecting and identifying such a "decoupled" nuclear explosion would thereby be increased.

These ideas have since received some experimental verification from the underground tests of project Cowboy [Herbst et al., 1961; Adams and Allen, 1961]. In these tests, extensive seismic data were obtained when high explosives were detonated at the center of two spherical cavities, of 6 ft (1.83 meters) and 15 ft (4.57 meters) radii, in a salt dome and also when tamped charges were exploded in the salt. Comparison of seismic signals from cavity and tamped explosions showed significant decoupling. In addition to the seismic data, a considerable body of measurement was obtained from the cavity explosions which record the close-in effects of wave propagation in the salt and the explosive blast pressures on the cavity wall [Murphey, 1961].

Although some theoretical calculations of events in the salt near the cavities have been compared with experiment [Herbst et al, 1961] and although independent calculations of the hydrodynamics inside the cavities have been carried out at Lawrence Radiation Laboratory [H. R. Nuckolls, private communication], as far as the authors are aware, no results of an entirely theoretical nature concerning both cavity hydrodynamics and close-in phenomenology in the salt have been published. Starting from first principles, theoretical calculations of the cavity hydrodynamics are used as the basis for a series of elastic wave calculations in order to obtain theoretical descriptions of the close-in elastic radiation field in the salt and the nonsteady flows in the cavities. These theoretical results are compared with experiment.

The nature of these results is such as to indicate some physical trends which might otherwise be obscured in empirical or purely experimental determinations. These calculations, when compared with experiment, permit the assessment of the precision of both elastic wave theory and of the theoretical hydrodynamic description of the cavity blast. We point also to some methods of correlating the experimental results which may previously have escaped notice.

CAVITY EXPLOSION THEORY

Explosive properties--loading density and equation of state effects. The initial density (loading density) of the explosive plays an important role in determining both the detonation properties and the final gas properties. Jones and Miller [1948] give compositions and equations of state for the gaseous products from TNT at loading densities of 1.5 and 1.0 g/cm^3. The gaseous products are remarkably different both at the Chapman-Jouget point (at the detonation front) and after expansion to low pressure. Pelletol was used in the Cowboy experiments. It consists of small spheres of solid TNT, which results in an over-all loading density of unity (ρ_e = 1.0 g/cm^3).

The detonation wave in center-detonated cast TNT (ρ_e = 1.5 g/cm^3) leads to a peak (Chapman-Jouget) pressure of about 160 kb, an energy density of about 5.3 x 10^{10} ergs/g, and a detonation velocity of 6.4 m/msec. This results in a temperature close to 3400°K and a compressed density of about 2.0 g/cm^3.

In contrast, the similar detonation front conditions in TNT of loading density unity (ρ_e = 1.0 g/cm^3) (Pelletol) give a pressure of about 82 kb, an energy density of about 4 x 10^{10} ergs/g, a detonation velocity of about 4.5 m/msec, a temperature of 3800°K and a density of about 1.42 g/cm^3. Thus less energy is released and a lower initial pressure is created in a given weight of explosive. In essence, it takes 1 1/3 kg of Pelletol to provide an energy release comparable to that from 1 kg of cast TNT.

In addition, the detonation product gases are different and behave differently on expansion. At densities close to normal air densities the effective adiabatic exponent (γ) is 1.27 for cast TNT, but it is 1.20 for the Pelletol. Since the average pressure from this gas in a cavity will be proportional to the energy density multiplied by the factor (γ-1), the difference for the two explosives is considerable. This effect is in addition to the effect of the lower initial energy release of Pelletol.

To insure a proper energy deposition on detonation and a correct detonation velocity, a burn routine was provided in the calculations which added energy at an appropriate rate in the few zones associated with the detonation front. The position of the front as a function of time was fixed by the detonation velocity, and the rate of energy deposition was dictated by the desired burn yield. The accompanying hydrodynamic conditions and equation of state then fixed the detonation pressure and compression. Once the detonation had burned out, the problem was reduced to one governed by hydrodynamics alone.

Several calculations were made to investigate the sensitivity of results to the burn conditions and to the equation of state. The importance of the air in the chamber (partially evacuated) was also investigated. Figure 1 compares the wall pressures for four calculations, all for 20 lb (9 kg) of explosive in a 6-ft-radius (1.83 meters) cavity. The highest reflected pressure occurs for the cast TNT (ρ_e = 1.5) reaching 570 lb/in^2 (39.3 bar). The rest are for calculations using Pelletol (ρ_e = 1.0). The sharpest and next highest pressure peak was for Pelletol, but instead of being burned

with a proper detonation wave, all the energy was dumped in uniformly with all velocities zero initially and with no initial compressions. In addition, this second case had a vacuum in the chamber (no air). A third calculation treated a proper detonation and included air in the chamber at 1/20 of normal air density. The last represented calculation (and the lowest peak reflected pressure) was also for a detonated Pelletol charge in 0.05 ρ_o air, but with a further alteration in the equation of state which changed the behavior of the specific heat along an adiabat.

These four calculations (Figure 1) still do not lead to an unambiguous comparison of the effect of detonation versus the effect of "no-burn" on the resulting wall pressure, and to remedy this, a comparison calculation was run both with and without burn for the case of 200 lb (90 kg) in a 15-ft cavity. A peak wall pressure of 39 bar resulted for the "no-burn" case followed by a very sharp drop to around 6.9 bar while the case including the detonation detail rose to a flatter peak at around 14.8 bar. These cases are compared in Figure 2. The peak pressures are obviously very sensitive to the detonation details, which is in some ways unfortunate, since more information about the explosives is then required than is normally available.

The short-dashed curve in Figure 2 represents the time-average of the wall pressure after shock arrival and up to each instant, i.e.

$$\langle P \rangle \equiv \frac{1}{(t-t_s)} \int_{t_s}^{t} P\,dt \qquad (1)$$

Equation of state for explosives. The equations of state for both forms of TNT were approximate fits to the adiabatic data of Tables 3 and 5 of Jones and Miller [1948] (modified so as to avoid negative slopes in the internal energy versus temperature). The resulting fits represent equations of state which are incorrect in detail but which produce the correct initial and "final" states, provided the influence of multiple shocks does not put the gases on adiabats of markedly different character. Since the larger charges do not expand to anything like normal air density in these small cavities, and since reflected shocks may be fairly strong, the proviso just injected is not always observed in these calculations; to that extent, then, the results at late times may suffer from lack of a more precise equation of state treatment.

The following approximate fit to the equation of state for Pelletol (P) was used, based on the adiabatic data of Jones and Miller [1948, Table 5].

$$P_p = \frac{T}{V}\left(2.89 + \frac{12.24}{.5+V^2}\right)X10^{-4} \qquad (10^{10}\ \text{ergs/cm}^3) \qquad (2)$$

where T is in ^{o}K and V is in cm^3/g.

$$E_p = \frac{.96T}{650+T^3X10^{-7}} + 1.655T^4X10^{-14} \qquad (10^{10}\ \text{ergs/g}) \quad (3)$$

The later ammended form appears as

$$E'_p = \frac{.96V'T}{650V'+T^3X10^{-7}} + 1.655T^4X10^{-14} \qquad (10^{10}\ \text{ergs/g}) \quad (4)$$

where V' is taken as unity for ρ greater than 1 g/cm^3 and as equal to the specific volume ($V = 1/\rho$) for ρ less than 1. The effect of this change was to reduce the effective gamma of the detonation products at intermediate temperatures and low densities (i.e. in the region of 1000° to $3000^{\circ}K$ and at densities less than the initial loading density). This form of the equation of state leaves the detonation front and the cold gas conditions unchanged for the detonation products. The effective (γ-1) or PV/E functions resulting from this (equation 4) and the earlier equation of state fit (equations 2 and 3) are illustrated in Figure 3, as functions of the temperature for fixed densities.

For cast TNT ($\rho_e = 1.5$), the fit used was based on Table 3 of the same reference.

$$E_T = \frac{7.73\ T}{8500+T^4 X10^{-13}} + 1.2T^5 X10^{-17} \qquad (10^{10}\ \text{ergs/g}) \quad (5)$$

$$P_T = \frac{2.556\ \Phi}{V}\left\{1 + \frac{\Phi^5}{10^{-4} + .141\ \Phi^4}\ (1.15 + 10.96\ \Phi - 288\ \Phi^2 + 2343\ \Phi^3 - 7800\ \Phi^4 + 9237\ \Phi^5)\right\} \qquad (10^{10}\ \text{ergs/cm}^3) \quad (6)$$

where $\Phi = TX10^{-4}$

Detonation characteristics. The actual burn rate is determined by the equation of state and loading density of the explosive. The Chapman-Jouget conditions which apply at the detonation front are quite different for the two TNT loading densities considered. For $\rho_e = 1.5$, and $\rho_e = 1.0\ g/cm^3$ the following values were required at the detonation front.

Table 1.

Detonation Characteristics for TNT and Pelletol

Physical Parameter	Units	TNT	Pelletol
Loading Density, ρ_e	gm/cm^3	1.5	1.0
Detonation Velocity, U_{CJ}	m/msec	6.507	5.00
Internal Energy, E_{CJ}	10^{10} ergs/g	5.447	4.074
Pressure, P_{CJ}	10^{10} ergs/cm^3	15.88	8.224
Density, ρ_{CJ}	g/cm^3	2.00	1.421
Temperature, T_{CJ}	^oK	3400	3800

Cavity air. When the cavity air was included (at various degrees of evacuation), its equation of state was determined in the calculations by the detailed fit given below. The equation of state of air is of some importance here, since the air around the explosive is compressed and heated well beyond a point where its behavior can be taken as that of an ideal diatomic gas.

For hydrodynamic calculations it is sufficient to consider only the caloric relation between the internal energy (E), the pressure (P), and the density (ρ) of the gas in question. Such an equation of state for air can be expressed in many ways; for convenience and simplicity of an analytic fitting the following form has been developed to cover all temperatures and a range of densities from 10 times the normal sea-level density of air to 10^{-6} normal density. The ideal gas relation, $E = P/\rho(\gamma-1)$, can be generalized to any equilibrium gas by appropriate definition of the proportionality constant $(\gamma-1)^{-1}$. The following fit agrees with RAND and National Bureau of Standards for air [Hilsenrath and Beckett, 1955; Gilmore, 1955] to within 5 per cent almost everywhere. If we define a quantity $\mu = (\gamma+1)/(\gamma-1)$, the pressure becomes

$$P = \frac{2\rho E}{\mu-1} \tag{7}$$

$$\mu = 1 + \frac{27y+3}{5y+1} + A + B + C + D + E + F + G + H + I \tag{8}$$

in which $$y \equiv \left(\frac{P_o}{P}\right)\left(\frac{\rho}{\rho_o}\right)^{1.0553} \quad \text{and} \quad \xi \equiv \ell n(\rho/\rho_o) \tag{9}$$

and the literal factors (A through I) have the form

$$Z = \frac{(X_o + X_1\xi + X_2\xi^2)y^m\,(1 - y)u}{(X_3 + X_4\xi)wy^n + 1} \tag{10}$$

Table 2 gives the values of the various coefficients for each term in μ. (In the table, the exponents of numerical coefficients indicate the powers of 10, e.g., 2.236^{+5} means 2.236×10^{5}.) The general nature of this fit to the equation of state for air is illustrated by Figure 4.

Computational method for explosion hydrodynamics. The gas dynamics of these spherical explosions finds mathematical description in a set of partial nonlinear differential equations. The technique used in the numerical integration of these equations is similar to previously reported Lagrangean formulations in which an artificial viscosity is used to treat shock waves [Von Neumann and Richtmyer, 1950; Brode, 1955; 1959]. An outline of the numerical method employed for the present cavity explosions is included as Appendix A, since much of the detail is not generally available elsewhere, and since an appreciation of the relative veracity of the solutions is most dependent on an understanding of the physical approximation embodied in the mathematical model.

Table 2. Factors in Equation 10

Z	A	B	C	D	E	F*	G	H	I
m	1	1	2	4	2	3	3	4	10
n	6	2	3	8	3	6	6	6	16
X_0	2.236^{+5}	4.975^{+4}	1.272^{+6}	3.892^{+7}	8.730^{+4}	4.890^{+9}	2.774^{+4}	1.547^{+10}	0
X_1	-1.509^{+4}	-5.463^{+3}	-1.246^{+5}	-2.295^{+7}	$+3.190^{+3}$	$+7.125^{+8}$	-7.849^{+3}	-1.671^{+8}	1.619^{+11}
X_2	0	0	-3.053^{+3}	0	0	0	0	-6.617^{+7}	0
X_3	5.412^{+27}	1.609^{+7}	2.615^{+7}	3.330^{+14}	4.976^{+5}	8.368^{+17}	3.243^{+7}	-8.490^{+9}	7.275^{+18}
X_4	0	0	1.034^{+6}	0	-1.883^{+3}	0	-5.494^{+6}	4.0^{+8}	0
u	1	1	1	1	1	1	1	$(1-y)^2(y-c)(y-d)$	1
w	1	1	100y+1	1	1	1	1	1	1

*ξ in numerator of F is absolute, i.e., $|\xi|$

$c = 7.4^{-2} - 3.764^{-3}\,\xi$ if $\xi \leq 0$

$c = 7.4^{-2} - 3.764^{-3}\,\xi - 5.852^{-3}\,\xi^2$ if $\xi > 0$

$d = 2.357^{-2} - 4.255^{-3}\,\xi - 2.52^{-4}\,\xi^2$

$s^{+t} = s \times 10^{t}$

CAVITY HYDRODYNAMICS

Results. The wall-pressure histories were extracted from these calculations to provide an input to the calculations of elastic wave propagation. These histories are illustrated in Figures 1, 2, and 5 through 9.

To indicate something more of the behavior of the blast in such a cavity, some pressure density and temperature profiles for the case of 20 lb (9 kg) in a 12-ft-diameter (3.66 meters) cavity are illustrated in Figures 10 through 12. Figure 10 displays pressure as a function of radius at various times after detonation. In it one can follow the expansion from a time near the end of the Pelletol burning ($t \sim 0.025$ msec) (where product gases have pressures near 100 kb) through the time when the wall pressure reaches a maximum and the reflected shock has begun its first implosion on the origin ($t \sim 0.78$ msec). At first ($t \sim 0.042$ msec) the expanding high-explosive product gases "snowplow" the rarefied ($P_o \sim 0.0509$ bar) air. But as the expansion proceeds ($t \sim 0.154$ msec), the compressed air begins to build up an excess pressure ahead of the expanding explosion products. As the restraint of the cavity wall is felt, the decelerating air and explosion product gases pile up a reflecting shock ($t \sim 0.527$ msec) and reach a peak reflected pressure at $t \sim 0.7803$ msec of 13 bars (188 lb/in^2).

As the pressure contour history continues, the first reflected shock is seen to implode, reflecting at the origin to cause a second shock at the wall (at ~ 3 msec), followed by several rather weak shock traversals.

The gas densities follow a similar history through the detonation and first reflection (Figure 11) but lead eventually to a hotter, lower density shell of air at the wall most noticeable at late times.

The temperatures are initially somewhat less than $4000^{\circ}K$ in the detonation products (Figure 12), cooling on expansion, but rising again on being compressed by the reflected shock. Note that the expanded gases drop to temperatures less than room temperature before jumping to around $3000^{\circ}K$ through the reflected shock. The implosion at the origin brings temperatures there of the order of $8000^{\circ}K$. This preferential heating leaves a temperature distribution at later times, but before mixing and gravitational effects become important. The air, compressed against the wall, is then hot ($\sim 4500^{\circ}K$) while the detonation product gases show a sharp rise from less than 3000° to a maximum at the origin close to $8500^{\circ}K$.

Since only the wall pressure histories are needed to define the elastic wave propagations, such more complete hydrodynamic descriptions for the other cases for which calculations were made have not been included. Table 3 represents a summary of the various conditions governing each of the calculations, as well as such information as the peak wall pressures, time intervals between first and second shock, approximate final wall pressure, length of time covered by the calculations, and appropriate figure numbers illustrating the wall pressure histories.

Table 3. Summary of Calculations

Cavity diameter (meters)	1.83	3.66							9.14			
Explosive type*	T	T	P	P	P′	P	P′	P′	P	P	P	P′
Charge weight kg	9	9	9	9	9	45	450	900	90	90	230	450
Charge weight lb	20	20	20	20	20	100	1000	2000	200	200	500	1000
Total Energy (10^{14} ergs)	--	--	3.4	3.8	3.8	1.8	190	460	43	37	93	190
Detonated	yes	yes	no	yes	yes	no	yes	yes	no	yes	yes	yes
Detonation velocity (m/msec)	5.7	5.7	--	3.8	3.8	--	4.5	5.0	--	3.8	3.8	4.5
Detonation energy density (10^{10} ergs/g)	5.45	5.45	4.07	4.07	4.07	4.45	4.07	4.6	4.78	4.07	4.07	4.07
Initial air pressure in cavity (mbar)	5.1	5.1	0	51	51	0	25	0	51	81	81	25
Peak wall pressure (bars)	~690	39	22	13	12	110	500	1010	39	15	52	66
Second peak pressure (bars)	--	--	7.2	7.3	4.8	41	200	303	7.3	6.1	13	12
Time interval between 1st and 2nd peak (msec)	--	--	2.21	2.32	3.06	2.23	3.47	2.4	5.63	6.07	6.60	8.5
Final pressure on wall (Avg) (bars)	--	--	3.9	47	3.4	19	138	253	3.5	3.2	6.5	8.2
Energy radiated (10^{10} ergs)	--	--	3.1	1.5	1.1	73	1620	7160	61	19	96	216
Duration of calculation (msec)	.20	1.0	13.0	4.94	5.5	20.0	7.5	15.4	13.0	13.4	52	56
Illustration figure numbers		1	1	1	1	5	6	7	2	2	8	9

*T = TNT, P = Pelletol, P′ = Pelletol, revised equation of state.

Comparison with measured cavity wall pressures. A comparison of these calculated wall pressures with the measured (gage) pressures may help to put in proper perspective the importance of the variables mentioned previously in connection with choices of boundary and detonation conditions, equations of state, and inclusion or exclusion of rarefied air. Figures 13, 14, and 15 offer comparisons for the 90-, 230-, and 450 kg shots in the 9 meter cavity. The data were obtained only crudely from photographic reproductions of the instrument recordings and are labeled according to the field station designations. No attempt is made here to interpret from these the gage type or location (other than at the cavity boundary) or to make any implications or interpretations on the basis of instrumentation details. (It should be reiterated that the data curves shown are inexact; for more precise data reproductions, reference to the original or direct copy tracings would be advisable.)

In Figure 13, two data records are indicated in comparison with two calculations. Of the latter, one is for Pelletol properly detonated, and the other is for Pelletol without burn (as in Figure 2). Beyond general similarities, one can discern that the second reflection occurs consistently earlier (by about 1 msec) for the calculated cases. The semilog scale of pressure should be recognized as overestimating the differences at low pressures (where the records are hard to resolve) and as underestimating the differences at high pressures (where the data records seem to suffer from extraneous zero-time transient signals).

Figure 14 compares the calculation for 230 kg in the 9 meter cavity with two pressure records, showing again a tendency in the calculation toward early second pulse arrival, or, more exactly, a shorter period of oscillation throughout. Early gage pressures seem to be higher except in the calculated first spike. This spike is not evident in the gage records. Aside from such obvious differences, the calculation appears to provide the general transient characteristics, as well as an appropriate average or late-time pressure value.

In Figure 15 comparison is made for 450 kg in the 9 meter cavity. Although the early-time comparison again shows higher measured pressures and no spike, the period for the calculation in this case appears to be longer than that evidenced by the data.

The period discrepancies may stem from a combination of inexactitudes: in both the calculations and the actual shots the charge weights and detonation conditions were not precise; for example, in the experiments the charges could not be exactly center-detonated nor could the explosive packing density be exactly controlled. Since the packing density can evidently affect the detonation velocity and energy release, the effective charge weight should be considered an approximate guide to the net explosion energy. Similarly, in the calculations, the detonation conditions were only approximately controlled, and detonated velocities and energy releases were neither precise nor constant. In view of the variations and vagaries in the calculations alone, the discrepancies in period and in peak values of pressure (of the order of 10 to 15 per cent) are not surprising.

But the calculated peak values of the second pulse seem to be too low, even on this loose scale of comparison. In the 230 kg case, the calculated second peak is 6.2 bar while the data curves range from 12.8 to 20.7 bar, and in the 450 kg case the data curves both reach 27.6 bar, while the calculation rises to less than 14 bar.

ELASTIC RADIATION CALCULATIONS

Calculations of spherically symmetric dilation waves resulting from a time-dependent pressure on the wall of a spherical cavity have been carried out with considerable generality by many writers [Eringen, 1957; Hopkins, 1960]. The present calculations were accomplished in a straightforward manner to describe the spherical elastic radiation field generated by the theoretical wall-pressure histories characteristic of the Cowboy cavity explosions. Before discussing these results we shall indicate the method by which they were calculated. The basic equations are presented below without derivation. A derivation of these particular equations is given by Parkin [1962].

Let a be the radius of the cavity, P(t) the pressure acting on the cavity wall, and aF(t) the radial elastic displacement at the cavity wall. The function F(t) is given by

$$F(t) = \frac{c^2}{a^2\omega}\frac{1}{\lambda+2\mu}\int_0^t P(\tau)\left[\frac{1-\beta}{2}\sin\omega(t-\tau) + \frac{a\omega}{c}\cos\omega(t-\tau)\right] e^{-\frac{1+\beta}{2}\frac{c}{a}(t-\tau)}\,d\tau \tag{11}$$

where

$$\omega = \frac{c}{2a}\sqrt{4 - (1-\beta)^2}$$

and

$$\beta = \frac{2\mu-\lambda}{2\mu+\lambda}$$

The quantities λ and μ denote the Lamé constants of the elastic material and c is the dilatational wave speed,

$$c = \sqrt{\frac{\lambda+2\mu}{\rho}} \tag{12}$$

The density of the medium is denoted by ρ. The radial strain $\epsilon_r(r,t)$, then, is given by

$$\epsilon_r = 2\frac{ac}{r^2}\left(1 - \frac{a}{r}\right) e^{-\frac{c}{a}\left(t - \frac{r-a}{c}\right)} \int_0^{t - \frac{r-a}{c}} e^{\frac{c}{a}\xi} F(\xi)\,d\xi \tag{13}$$

$$+ \frac{a}{r}\left(1 - 2\frac{a}{r} + \beta\right) F\left(t - \frac{r-a}{c}\right) - \frac{a}{r}\frac{1}{\lambda+2\mu} P\left(t - \frac{r-a}{c}\right)$$

The transverse strain ϵ_θ is given by

$$\epsilon_\theta = -\frac{ac}{r^2}\left(1 - \frac{a}{r}\right) e^{-\frac{c}{a}\left(t - \frac{r-a}{c}\right)} \int_0^{t - (r-a)/c} \exp(c\xi/a) F(\xi)\,d\xi + \frac{a^2}{r^2} F\left(t - \frac{r-a}{c}\right) \tag{14}$$

From these results one can compute the radial elastic displacement $u(r,t) = r\epsilon_\theta$, the dilatation $\epsilon_r + 2\epsilon_\theta = \Delta(r,t)$, and the two stress components

$$\sigma_\theta = \lambda\epsilon_r + 2(\lambda+\mu)\epsilon_\theta$$

and (15)

$$\sigma_r = (\lambda+2\mu)\epsilon_r + 2\lambda\epsilon_\theta$$

The particle velocities and accelerations are obtained by differentiating the formula for $u(r,t)$ with respect to time.

All the preceding formulas were programmed for RAND's Johnniac digital computer. Numerical values for the stresses, strains, dilatation, particle displacement, particle velocity, and particle acceleration were calculated as functions of time, t, at any radius, r, from the center of the cavity.

In conjunction with the spherical wave code outlined above, a short Fortran code has been written for the spectral analysis of the particle velocities. This program calculates the quantity

$$F(\omega) = \left| \int_{-\infty}^{+\infty} u_t(t) e^{-i\omega t} dt \right| \tag{16}$$

In addition to the machine calculations noted above, hand calculations were made to obtain the total energy radiated into the elastic medium.

Imagine a volume V of the elastic medium which moves solely by the deformation of the material. The energy flux W radiated through the surface S of this volume is equal to the rate at which the stresses on S do work upon the material outside V [Thomas, 1961]. If the time interval T includes the total pulse duration, we can write the approximate result for spherically symmetric motions so that

$$W = 4\pi r^2 \int_0^T u_t \, \sigma_r dt \tag{17}$$

where it is assumed that $r(r_o,t)$ can be replaced by r_o. This Lagrangean formulation does not include any transport terms.

The elastic constants used in the calculations indicated above are

Young's modulus, E = 353.4 kb

Poisson's ratio, = 0.25

Dilatation wave speed, c = 4.39×10^3 m/sec

After the present calculations were started, Nicholls et al. [1960] published slightly different definitive values. The present values, however, appear to be close enough to those cited so that no further calculations are necessary.

Calculations were carried out for cavity radii of 1.83 and 4.57 meters corresponding to ten of the twelve hydrodynamic calculations. The two cases for explosions of cast TNT were excluded from further study, as they were calculated for time intervals too short to be of present use. For each theoretical P(t) from these Pelletol explosions, elastic wave calculations were run for three radii which were chosen to approximate closely the experimental gage locations. Thus, for the 1.83 meter cavity, r values were chosen to be at 3.05, 6.31, and 11 meters from the center of the cavity. For the 4.57 meter cavity, chosen r values were 7.62, 15.4, and 24.4 meters.

THEORETICAL AND EXPERIMENTAL RADIATION DATA

As explained above, the hydrodynamic conditions within the cavity are markedly influenced by the nature of the burning process and by the equation of state for the explosive products. These effects are directly mirrored by the response of the elastic medium, as evidenced by the large variations in radiated energy of Table 3 for the same charge weight but for the different equations of state for the explosive. Of course, the calculated values of the radiated energy depend upon the time interval over which the calculation is extended. Even for those cases of longest duration it is not strictly true that the entire elastic pulse could be used in (17). On the other hand, it was found that the calculations of shortest duration contain about 90 per cent of the radiated energy. The calculations of greatest duration appear to give energy values which are accurate to within 1 per cent.

Figures 16 and 17 compare particle velocities in the salt after detonation of 90- and 230- kg Pelletol charges. As noted previously, these theoretical curves result from using the values of wall-pressure versus time from Figures 2 and 8 as input data for the elastic wave program. Figures 18 and 19 compare particle velocities and particle displacements at two distances from the center of the 4.57 meter cavity corresponding to the theoretical P(t) curve of Figure 9 for a charge weight of 450 kg. The two radial distances are 7.62 and 24.4 meters, respectively.

The over-all agreement between experiment and theory shown by these four illustrations is thought to be quite satisfactory. The differences between theoretical and experimental values of peak wall pressure from the cavity hydrodynamics appear here as corresponding differences in peak particle velocities. The somewhat better agreement between experiment and theory for the magnitudes of subsequent peaks as well as the improved correlations of the time intervals between peaks is also noted in the wall-pressure curve. In Figure 19 the difference between the experimental and theoretical arrival times from the instant of detonation until reception of the first signal is about 1 msec at r = 24.4 meters. Figure 18 and the wall-pressure curves of Figure 9 indicate that this difference should be about 1/3 msec. Inspection of the "digitized" velocity data [Adams and Allen, 1961] at r = 24.4 for shot 10 of the Cowboy tests tests indicates agreement with the 1/3 msec figure.

The experimental data of Figures 16 through 19 of this paper have been taken from copies of the oscillograph recordings which were made from the original taped records. Evidently the detonation time marked on the particular record at r = 24.4 meters has been inadvertently misplaced. Had we made use of this information in Figure 19, the agreement between experiment and theory would have been greatly improved. However, we have applied no corrections to the experimental data. The experimental displacement data of Figures 18 and 19 have been read from records that were obtained from the velocity tapes by a process of electronic integration. [Murphey, 1961]. Comparison of experimental and theoretical displacement curves indicates the possibility of some drift in the

experimental records. It is to be noted that Herbst et al.[1961] present an experimental displacement curve in Figure 19 of their paper which corresponds to the conditions of our Figure 19. Their experimental curve results from the integration of the velocity record (presumably by direct numerical computation) and does not show any drift. Use of their curve in Figure 19, instead of that read from the electronically integrated record, would provide excellent agreement between experiment and theory for particle displacements at $r = 24.4$ meters.

Figure 20 compares velocity spectrums calculated from the experimental and theoretical velocity data of Figures 18 and 19. At high frequencies these spectrums show fair agreement. The pulsation frequency of the gas in the cavity is clearly shown by the peak in these curves between 100 and 200 cps. The spectrums calculated from the measured velocities have considerably greater low-frequency content than the theoretical spectrums. Investigation of this difference indicated that it was partly due to the fact that the experimental velocity curves of Figures 18 and 19 have been drawn with rather broad initial peaks. Actually, as already discussed by Murphey [1961], the velocity records of the decoupled shots showed a high-frequency component due to ringing of the cannisters containing the gages. Although this high frequency on the recordings is of fairly small amplitude, it obscures the width of the initial velocity pulse. In the process of trying to smooth out these oscillations in drawing the experimental curves, the width of the initial pulse tends to be overestimated.

For example, when a somewhat narrower initial pulse was obtained from a rereading of the data of Figure 18, the low-frequency part of the experimental curve of Figure 20 was lowered by about a factor of 2. No attempt has been made to improve the agreement between experiment and theory by applying this factor because of the uncertainties associated with such procedures.

Another cause for disagreement between the experimental and theoretical spectrums resides with the truncation of the records which were analyzed. For consistency, all curves of Figure 20 were calculated for 20 msec after the arrival time for the velocity function u_t in (16). Outside this 20 msec interval the velocity is assumed to vanish. On the other hand, when the record is truncated at some arbitrary time T later than the arrival time, (16) shows for low frequencies ($\omega = 0$, to be exact) that $F(\omega)$ is nearly equal to the particle displacement $u(T)$. If the interval of time used in (16) is short enough, $u(T)$ can show considerable variation, depending upon the choice of T. The largest variation in $F(\omega)$ resulting from this cause was found to be within 30 per cent at $\omega = 0$.

The preceding comparisons have been made for experimental conditions in which the assumptions of elasticity are reasonably well satisfied. For the larger-yield explosions in the smaller sphere, the salt shows an anelastic behavior, which can be illustrated clearly by a comparison of experimental and theoretical results. For this comparison it seems sufficient to compare peak values of the particle velocity and of the particle displacement for each case. The various values are entered in Table 4. Nearly all of the experimental values

given in Table 4 have been reported by Murphey [1961] in his Tables 3 and 4.[1] The first thing indicated by Table 4 is that the peak velocities and displacements deduced from the Pn calculations show considerable differences from the experimental quantities, while the values calculated from the Pb and P'b wall pressure functions are in fair or good agreement with experiment. A second thing revealed by these data is that, for those cases in which elasticity of the salt is a good approximation, the agreement between experiment and theory seems to be best at those radii closest to the center of the cavities. Comparison of trends at greater ranges appears to indicate that, even for small strains, the salt has an element of dissipation that is not accounted for by the theory . Finally, the effects of plasticity or other anelastic behavior are shown dramatically by the results from the "overdriven" cavity of 1.83 meter radius with the 900 kg charge.

Comparisons between experimental and theoretical data for other physical quantities are possible. The preceding comparisons, however, seem to be the most useful ones at this time. For example, the particle acceleration data from the tests show exceedingly large variations from the theoretical values, and the body of these measurements does not appear to be internally consistent. Similarly, the data from the "earth-pressure" gages (whatever it is they measure) show great scatter among themselves, and these pressures show no resemblance to calculated values of σ_r, σ_θ or $\sigma_r - \sigma_\theta$. Unfortunately, $\epsilon_r(t)$ data from the dynamic strain gages [Nicholls et al., 1960] were obtained for r values that were considerably larger than any radius used in present calculations.

---

[1] In Table 4 of Murphey [1961] shot 3 should be designated as shot 2 and shot 4 should be designated as shot 3.

Table 4. Experimental and Calculated Peak Particle Velocities and Displacements

Shot No.	Range (M)	Gage No.	Peak Particle Velocities (cm/sec)				Peak Particle Displacements (μ)			
			Measured	Calculated			Measured	Calculated		
				P'b	Pb	Pn		P'b	Pb	Pn
	3.05			5.05	5.2	11.6		17	19	19
2	6.31	1.1-2-V	1.8	2.18	2.24	5.3		6.9	7.6	7.9
(20 lbs)	11.0	1.1-1-V	1.3	1.19	1.22	3.0		3.8	4.1	4.3
6'	11.0	1.1-6-V	1.1	1.19	1.22	3.0		3.8	4.1	4.3
	3.05					62				106
3	6.31	1.1-5-V	8.6			29				44
(100 lbs)	6.31	1.1-2-V	5.3			29				44
6'	11.0	1.1-1-V	3.3			16				24
	11.0	1.1-6-V	4.8			16				24
	3.05			254				630		
12	6.31	1.1-5-V	81	120			540	240		
(1000 lbs)	6.31	1.1-2-V	62	120			410	240		
6'	11.0	1.1-1-V	32	68			170	130		
	11.0	1.1-6-V	27	68			200	130		
	3.05			518				1380		
14	6.31	1.1-5-V	180	238			1320	540		
(2000 lbs)	6.31	1.1-2-V	140	238			1090	540		
6'	11.0	1.1-1-V	67	134			470	290		
	11.0	1.1-6-V	69	134			480	290		
5	7.62				7.3	20			35	44
(200 lbs)	15.4	2.1-2-V	3.6		3.4	9.4	13.5		16	20
15'	24.4	2.1-1-V	1.1		2.1	5.9	6.4		9.4	12
	7.62	2.1-4-V	5.6		7.3	20	36.6		35	44
6	15.4	2.1-2-V	2.5		3.4	9.4	12.7		16	20
(200 lbs)	24.4	2.1-1-V	1.0		2.1	5.9	6.35		9.4	12
15'	24.4	2.1-6-V	1.0		2.1	5.9	6.6		9.4	12

Shot No.	Range (M)	Gage No.	Peak Particle Velocities (cm/sec				Peak Particle Displacements (μ)			
			Measured	Calculated			Measured	Calculated		
				P'b	Pb	Pn		P'b	Pb	Pn
8 (500 lbs) 15'	7.62	2.1-4-V	19.8		31		63.5		70	
	15.4	2.1-2-V	9.6		15		30.5		28	
	15.4	2.1-5-V	8.6		15		30.5		28	
	24.4	2.1-1-V	5.1		9.4		14.0		14	
	24.4	2.1-6-V	4.1		9.4		12.7		14	
10 (1000 lbs) 15'	7.62	2.1-4-V	33	39			127	117		
	15.4	2.1-5-V	13	19			46	43		
	15.4	2.1-2-V	15	19			53	43		
	24.4	2.1-1-V	6.6	12			23	25.4		
	24.4	2.1-6-V	6.1	12			15	25.4		

P'b (revised Pelletol, detonated)

Pb (Pelletol, detonated)

Pn (Pelletol, not detonated)

For this reason, no direct comparison between theoretical and measured radial strains is possible. Even so, the rise times for the experimental strains appear to be considerably longer than those that would be found from elastic calculations. This finding supports the evidence from Table 4 concerning the effect of dissipation at small strains in the salt.

CORRELATIONS FOR CLOSE-IN EFFECTS

The complex nature of the sequence of events inside the cavity makes it difficult to find useful ways of correlating characteristic features of the waves in the salt. However, if such a systematization of the data can be achieved, the theoretical findings, which are free of extraneous influences, should offer the greater chance of success. Even if such correlations are found, it is important to remember that they will be based upon the approximation that salt is an elastic solid. In situations for which the preceding results have shown that this is not actually a good approximation for salt, the fiction of elasticity is maintained below because of its theoretical interest.

Table 3 permits the comparison of the energy released by the explosions to that radiated into the salt. A significant feature of these results is that the radiated energy W is always a very small fraction of 1 per cent of U, the explosive energy released. To obtain a graphic idea of this result, one can represent W as a function of U in a log-log plot to find that the radius of the cavity, a, and the nature of the burn calculation for the explosive affect the result. Otherwise the radiated energy appears to be proportional to a constant power of the explosive energy. It is found that the radiated energy decreases as the cavity radius increases, so that one is led to plot W as a function of the ratio U/a. The result of this plot is shown in Figure 21 where now only data corresponding to explosions with or without detonation calculations lie on separate lines. Actually the data for the modified equation of state (P') lie on or below the solid

line in Figure 21, while the data for the equation of state designated by P are above the line, so that even in this case some differences in the details of the burn are evident. However, as noted previously, the limited accuracy of the calculations for the radiated energy W does not permit a definite distinction between these two cases. The curves of Figure 21 suggest that for detonated Pelletol we have, approximately,

$$W = 0.6 \times 10^{-12} (U/a)^{1.81} \text{ ergs} \qquad (18)$$

and for the (Pn) calculations, which exclude detonation, we have, approximately,

$$W = 2 \times 10^{-12} (U/a)^{1.81} \text{ ergs} \qquad (19)$$

for which U/a is expressed in dynes.

Because the elastic constants of the solid were not varied in the present theoretical calculations, it is not surprising that the preceding correlation shows no explicit dependence upon these constants. On the other hand, when the elastic constants for salt were used in an effort to obtain dimensionless correlations in accordance with the well-known laws of similitude [Parkin, 1958], no correlation of these results was found. For this reason, calculations for solids with different elastic constants, but for the same hydrodynamics inside the cavity, might be of considerable help in obtaining a more general result.

Although the radiated energy W appears to be simply related to the energy released by the explosive U, the essentially different magnitudes of these two quantities suggest that two characteristic

lengths might be significant for the dynamic response of spherical cavities. Thus, for effects associated with the explosion itself, we define a characteristic length,

$$\alpha = (U/E)^{1/3} \tag{20}$$

and for events out in the elastic medium we define another characteristic length,

$$\beta = (W/E)^{1/3} \tag{21}$$

(The length β is not to be confused with the parameter β defined previously in connection with equations 11 and 12.)
The Young's modulus E is taken as a characteristic pressure for both α and β even though it might seem more appropriate in the case of α to use a pressure characteristic of the explosive. Again we note that the elastic constants of the solid have not been varied in these calculations, so that the use of E in (20) and (21) secures only dimensional consistency.

The characteristic lengths α and β are useful for graphical presentations of the peak values of calculated quantities. For example, Figure 22 is a dimensionless plot of peak displacements versus the distance from the center of the cavity. The open points denote results calculated from the P'b equation of state, the solid point symbols indicate results from the Pb calculations, and symbols which are half solid and half open designate Pn results. This symbolism has been employed for Figures 23, 24, and 25 also. Figure 22 is the only instance in which it was found possible to achieve a

reasonably close correlation of the calculated results in terms of dimensionless quantities. For example, in Figure 23 it was necessary to plot the product of peak particle Mach number u_t/c and β^{-1} against the scaled distance r/α. Similarly, in Figure 24 the best over-all correlation is obtained when the product of dimensionless acceleration $u_{tt}\beta/c^2$ and β^{-2} is plotted versus scaled range. In this last case the correlation is not as good as that obtained in the two preceding examples. In Figure 25 the peak radial stresses, including the peak cavity wall pressures, are shown as a function of scaled range. The most efficacious combination of parameters for this correlation was found to be $\sigma_r/E\beta$.

In view of the difficulties involved in the scaling of single peak values of the various quantities studied, it is thought that the results given above constitute fairly good correlations. The fact that the points from the Pn calculations fall among the points from the Pb and P'b calculations is most encouraging. Because the system contains two characteristic lengths, the task of finding such trends is rather tedious, and we have not explored all possible combinations. Furthermore, considerations of similitude [Parkin, 1958] indicate that dimensionless quantities such as u/β, u_t/c, $u_{tt}\beta/c^2$, and σ_r/E are the appropriate parameters for such correlations, and these quantities have been employed even though the elastic constants have not been varied in the present study. For the same reason, these parameters have been retained even when it was not possible to obtain correlations with respect to these dimensionless quantities.

From the foregoing we see that if the dimensionless quantities u/β, u_t/c, and $u_{tt}\beta/c^2$ are multiplied by the quantity β^{-n} (where n = 0, 1, or 2 for the peak displacements, velocities, or accelerations, respectively), these quantities appear to be inversely proportional to the dimensionless range r/α. For the dimensionless radial stress, the appropriate value for n is unity.

The only data available to test the utility of the present correlation schemes consist of the measured peak particle displacements and velocities of Table 4. In the absence of experimental measurements for the energy radiated into the salt, we have calculated a value for each shot of the Cowboy tests as follows: First, the explosive energy U for each charge was calculated by using the value of 4.074×10^{10} ergs/g for the energy density of Pelletol. Then (18) was used to calculate the radiated energy W. The appropriate values of α and β for each shot follow from (20) and (21). With the help of these data and the sound speed in the salt, the experimental data of Table 4 can be characterized in terms of the parameters u/β, $u_t/c\beta$, and r/α. Plots of these quantities appear in Figures 26 and 27. The correlation of these data appears to be quite good. It suggests approximate power-law relationships of the form

$$u/\beta = 2.1(r/\alpha)^{-1.8} \tag{22}$$

and

$$u_t/c\beta = 0.186(r/\alpha)^{-1.3} \text{ per meter} \tag{23}$$

It is interesting to note that the experimental data show a more pronounced attenuation of peak scaled particle displacement and velocity with increasing scaled range than do the corresponding theoretical results. The theoretical values appear to be approximated simply by an inverse proportionality. Two factors that are probably responsible for this difference are those of plasticity and of other dissipation in the salt which occurs even at small strains. The first of these factors is most important at small scaled ranges. For a given explosive energy, plasticity in the salt permits larger particle displacements and velocities than would be obtained if the salt were truly elastic. The dissipation at small strains is most effective at large scaled ranges where it tends to diminish the magnitude of the peak displacements and velocities more strongly than it would in an elastic material. Of course, the calculation of the characteristic length β has been carried out under the supposition that the salt is an elastic material. To the extent that the salt departs from this idealized behavior, the results of Figure 18 are inaccurate. Moreover, the use of theoretical values of the radiated energy instead of measured ones is also a source of error. Nevertheless, Figures 26 and 27 serve to illustrate, in a fairly quantitative way, how wave propagation in the halite of the Cowboy tests differs from that which would take place in an elastic solid.

CONCLUSIONS

For the explosion phenomena within the cavities the following features were investigated and found to have significant influence on cavity wall pressures: (1) loading density of explosive, (2) equation of state of explosive products and of air, (3) the presence of air in the cavity, and (4) detonation details of explosion initiation and burn.

To a similar extent, the control of these same features must inevitably influence the actual experiments. Although great care went into the experiments to control and to record as many features of the explosions as practical, the very nature of explosives and detonations is in conflict with notions of precision and exact reproducibility, to the end that when coupled with the necessary instrumentation, uncertainties and comparisons of wall pressure measurements with calculated wall pressures for any one shot are not easily interpretable. In addition, several other "non-ideal" effects were of necessity present in the experiments: The initiations were only approximately central, and not entirely spherically uniform. The existence of supporting platforms and tripods together with packing material in the top of the plastic explosive containers may have added to the lack of symmetry.

The influences of a few important features of such an explosion have been investigated here, and it is hoped that an appreciation of these factors may aid both in the interpretation of these experiments and in the planning of future explosives tests.

The calculations of elastic waves presented here complete our attempt to give a wholly theoretical set of calculations for the cavity explosion phase of the Cowboy program. In view of the highly idealized theoretical model and of the uncertainties concerning the properties of the explosives used in the tests, the over-all agreement between close-in experimental measurements and theoretical calculations is thought to be excellent. Of course, those explosions which seriously overstressed the cavities must be excepted. These overdriven cavity examples when compared with the corresponding elastic calculations, give a good indication of the close-in effects of non-elastic response. Even in those cases for which the assumption of elasticity is a good approximation, comparison of experimental and theoretical trends has indicated some dissipative effects in the salt which are not present in an elastic material. Finally, the theoretical calculations have indicated the existence of some correlations between (1) explosive energy and radiated elastic energy and (2) close-in distances and the peak elastic displacements, velocities, accelerations, and radial stresses. These correlations could be of considerable use for predictions of these quantities for other cavity explosions in elastic materials. Before this potential usefulness can be reliably exploited, however, additional calculations should be carried out for the same and other explosive sources in other elastic materials in order to generalize the present findings.

Furthermore, we note that the correlations of experimental dimensionless peak particle displacements and scaled peak particle

Mach numbers with scaled range, although most encouraging, would be much more meaningful if they were based upon experimental values of the radiated energy. The fundamental importance of the radiated energy should make its experimental determination an essential part of future cavity explosion experiments. In such experiments, in elastic or anelastic solids, the fundamental quantity is the energy radiated from the surface of the cavity. Therefore, if one can measure the velocity of the cavity wall (or a particle velocity in the solid sufficiently near the wall) as a function of time, this datum together with the wall pressure history will permit a determination of the radiated energy. We hope that a feasible experimental technique for this determination will be found.

Appendix. COMPUTATIONAL METHOD

The problem presented by explosions lies in the solution of a set of nonlinear, partial differential equations representing the conservation of mass, momentum, and energy. These conservation laws may be expressed mathematically in several ways, but they are generally formulated in terms of either Eulerian or Lagrangean coordinates. The Eulerian form is an expression of the conservation laws as viewed from coordinate systems fixed in space, and the Lagrangean form is an expression of the same conservations in terms of a fixed set of masses or gas particles, so that a solution in the Eulerian case represents the history of the blast wave at a fixed point and a solution in the Lagrangean system describes the experience of a particle (or a volume of gas) as it moves about. The latter description is particularly fitting to this problem since the burning of an explosive is most easily described in terms of the history of each burning mass.

The set of equations below is one representation of these conservation laws in a Lagrangean system for a spherically symmetric explosion. In these equations the Lagrangean variable or mass coordinate is characterized by the mass per steradian; i.e., $m = \rho_1 R_o^3/3$ where ρ_1 is the initial density of the gas and R_o is its initial position.

$$\frac{1}{\rho} = V = \frac{1}{3}\frac{\partial R^3}{\partial m}\,, \qquad \text{conservation of mass;} \qquad (A1)$$

$$\frac{\partial u}{\partial t} = -R^2\frac{\partial}{\partial m}(P + Q)\,, \qquad \text{conservation of momentum;} \qquad (A2)$$

$$\frac{\partial E}{\partial t} = -(P + Q)\frac{\partial V}{\partial t} + D \,, \qquad \text{conservation of energy;} \qquad (A3)$$

$$E = E(T,V),\ P = P(T,V)$$

or $$\text{equations of state;} \qquad (A4)$$

$$P = P(E,V),\ T = T(E,V)$$

$$u = \frac{\partial R}{\partial t} \,, \qquad \text{particle velocity.} \qquad (A5)$$

In these equations the symbols are defined as follows:

V, specific volume

R, radial distance

u, particle velocity

P, pressure

Q, artificial viscosity pressure

E, specific internal energy

T, temperature

D, specific energy source (or loss) rate

m, mass/steradian

t, time.

In solving these equations for a specific set of initial and boundary conditions by numerical means, the usual approach is to arrange a set of difference equations which approximate these differential equations over a set of finite mass elements. In such a system, then, derivatives become differences, and a solution is accomplished by the repetition of a prescribed series of numerical steps which solve the difference equations for new values of the parameters which would occur after a small time increment.

To formalize the differencing procedure, consider the transformation of the above differential equations to another set in which the independent variables are a dimensionless Lagrangean coordinate j and a dimensionless time n, and in which the masses are represented by integer values of j and the time by integer values of n.

The Jacobian for the Lagrangean coordinate system then follows from the differential equation representing conservation of mass:

$$\frac{\partial m(j)}{\partial j} = \frac{1}{3V(j,0)} \frac{\partial}{\partial j} \left[R(j,0)\right]^3 = \frac{1}{3V(j,n)} \frac{\partial}{\partial j} \left[R(j,n)\right]^3 \qquad (A6)$$

The other conservation equations become

$$\left(\frac{\partial t}{\partial n}\right)^{-1} \frac{\partial u}{\partial n} = - R^2 \frac{\partial}{\partial j} (P + Q) \left(\frac{\partial m}{\partial j}\right)^{-1} \qquad \text{(momentum)} \qquad (A7)$$

$$\frac{\partial E}{\partial n} = - (P + Q) \frac{\partial V}{\partial n} + D \left(\frac{\partial t}{\partial n}\right) \qquad \text{(energy)} \qquad (A8)$$

and

$$u = \frac{\partial R}{\partial n} \left(\frac{\partial t}{\partial n}\right)^{-1} \qquad (A9)$$

In these equations the dependence of the variables on j and n has been suppressed for simplicity.

The artificial viscosity may be variously defined, but the following is a usual form:

$$Q = \frac{C}{V} \left(\frac{\partial u}{\partial j}\right)^2 \text{ if } \frac{\partial u}{\partial j} < 0$$

$$Q = 0 \qquad \text{if } \frac{\partial u}{\partial j} \geq 0 \qquad (A10)$$

in which the value of C determines the amount of spreading of shocks. When C is unity, the spread is about three zones, and when C is six the spread is around six zones, the constant being proportional to the square of the spread [Von Neumann, 1950; Brode, 1955].

In some unusual circumstances this form fails to provide the necessary shock spreading. Such a case can arise in some problems involving imploding shock waves.

A more rigorous form for the artificial viscosity, which is generally equivalent to the form above (equation A10), is the following:

$$Q = \left(\frac{\partial m}{\partial j}\right)^2 \frac{C}{R^4 V} \left(\frac{\partial V}{\partial n}\right)^2 \left(\frac{\partial t}{\partial n}\right)^{-2} \qquad \text{(A11)}$$

$$\text{for } \frac{\partial V}{\partial n} < 0$$

$$Q = 0 \text{ for } \frac{\partial V}{\partial n} \geq 0$$

The formation of a set of centered difference equations is now a matter of assigning integer values to the independent variables j and n and either defining the dependent variables at these points or at midpoints (at half-integer points) in j or n. It is conventional to express the j and n values associated with a given parameter by subscripts and superscripts; thus the radius at a mass point j and at a time t after n time increments $\Delta t(n) = \Delta t_n$ would appear as R_j^n.

The equations for the nth time step $\Delta t^{n+\frac{1}{2}}$ over a set of mass elements $\Delta m_{j-\frac{1}{2}}$ follow.

$$u_j^{n+\frac{1}{2}} = u_j^{n-\frac{1}{2}} - \frac{\Delta t^n}{\Delta m_j} \left(R_j^n\right)^2 \left[P_{j+\frac{1}{2}}^n - P_{j-\frac{1}{2}}^n + Q_{j+\frac{1}{2}}^{n-\frac{1}{2}} - Q_{j-\frac{1}{2}}^{n-\frac{1}{2}}\right] \qquad \text{(A12)}$$

for which $$\Delta m_j = \frac{1}{2}\Delta m_{j+\frac{1}{2}} + \frac{1}{2}\Delta m_{j-\frac{1}{2}}$$

and $$\Delta t^n = \frac{1}{2}\Delta t^{n+\frac{1}{2}} + \frac{1}{2}\Delta t^{n-\frac{1}{2}}$$

$$R_j^{n+1} = R_j^n + u_j^{n+\frac{1}{2}}\,\Delta t^{n+\frac{1}{2}} \tag{A13}$$

$$V_{j-\frac{1}{2}}^{n+1} = \frac{R_j^{n+1} - R_{j-1}^{n+1}}{3\Delta m_{j-\frac{1}{2}}}\left[(R_j^{n+1})^2 + (R_j^{n+1})(R_{j-1}^{n+1}) + (R_{j-1}^{n+1})^2\right] \tag{A14}$$

$$Q_{j-\frac{1}{2}}^{n+\frac{1}{2}} = C_1 \frac{\left[u_j^{n+\frac{1}{2}} - u_{j-1}^{n+\frac{1}{2}}\right]}{V_{j-\frac{1}{2}}^{n+1} + V_{j-\frac{1}{2}}^{n}} \quad \text{for } u_j^{n+\frac{1}{2}} < u_{j-1}^{n+\frac{1}{2}} \tag{A15}$$

$$Q_{j-\frac{1}{2}}^{n+\frac{1}{2}} = 0 \quad \text{for} \quad u_j^{n+\frac{1}{2}} > u_{j-1}^{n+\frac{1}{2}}$$

$$E_{j-\frac{1}{2}}^{n+1} = E_{j-\frac{1}{2}}^{n} - \left(\frac{1}{2}P_{j-\frac{1}{2}}^{n+1} + \frac{1}{2}P_{j-\frac{1}{2}}^{n} + Q_{j-\frac{1}{2}}^{n+\frac{1}{2}}\right)\left(V_{j-\frac{1}{2}}^{n+1} - V_{j-\frac{1}{2}}^{n}\right) + D_{j-\frac{1}{2}}^{n+\frac{1}{2}} \tag{A16}$$

In these equations it is worth noting that the quantities are either defined or averaged in such a way that first-order errors in Δt or Δm are avoided; i.e., the difference equations are centered. The actual progression of the solution can better be illustrated by reference to a space-time grid, as below, showing the points at which the various parameters are defined.

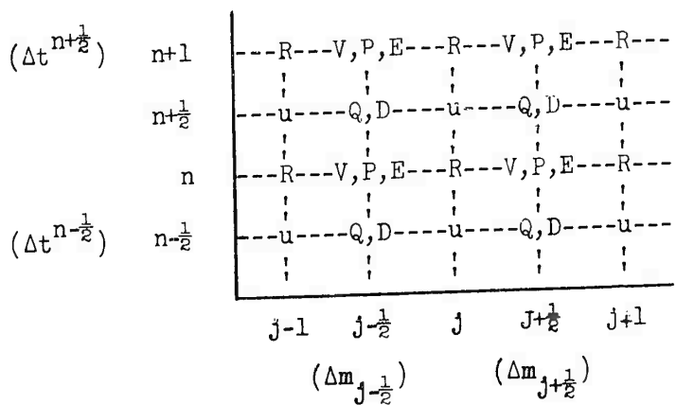

For illustration, assume that the nth time step has been completed, that, therefore, all the values at times less than n are known, and that the next step is to determine the values at $n+\frac{1}{2}$ and n+1 times. The difference equations have already been written in the order in which they are computed. The first equation defines a new velocity at time $n+\frac{1}{2}$, at point j, in terms of the old velocity at that j point at time $n-\frac{1}{2}$, and the radius at that j point at time n, together with the pressure gradients at that point and at time n as represented by the differences in the pressures at j points one half a unit on either side of j. From this new velocity a new radius is computed in a straightforward manner, using the definition of the particle velocity. These new radii, in turn, are used to compute a new specific volume, and that new volume together with the new values of the velocity can be used to compute a new artificial viscosity. The artificial viscosity is nearly of second order in the time, and its lack of symmetry in the velocity equation does not disturb the degree of accuracy of these otherwise centered difference equations. The new volume, together with the new artificial viscosity, can then be used in the energy equation to determine a new energy and a new pressure. If the equation of state is not simple, it is then necessary to arrive at the new energy and pressure by some iterative method. The equation of state represents a second relation between these remaining two unknowns, i.e., the new energy and the new pressure. With a satisfactory solution for all of these parameters at a point j one can then advance to the next j point and repeat the same procedure.

Of course, if the problem involves other mechanisms of energy transfer, or sources or sinks of energy, the term D in the energy equation becomes useful. For instance, the D term can be used satisfactorily in detonation wave calculations. A number of forms to represent the burning of high explosives or gases in a detonation front are possible; one fairly crude but workable form is the following:

$$D_{j-\frac{1}{2}}^{n+1} = \frac{E_{Cj}\Delta t^{n+\frac{1}{2}}}{t_{Cj}} \qquad (A18)$$

$$t_{Cj} = \frac{S\,\Delta R_{j-\frac{1}{2}}}{U_{Cj}}$$

in which E_{Cj} is the Chapman-Jouget energy, i.e., the energy generated in the detonation, U_{Cj} is the detonation velocity, and S is the spread or thickness of the detonation front in keeping with the shock spreading characteristic of the artificial viscosity technique.

A great many cautions resulting from experience and from the details of the handling of the numerical procedure might well be included in a complete description of a numerical method, since many special considerations are necessary before a numerical program becomes truly workable. Some of these factors are concerned with the stability of the numerical procedure, attention to boundary conditions and initial conditions, and internal checks on the accuracy of the computation. Such detail, however, is not considered appropriate to the completeness of this paper.

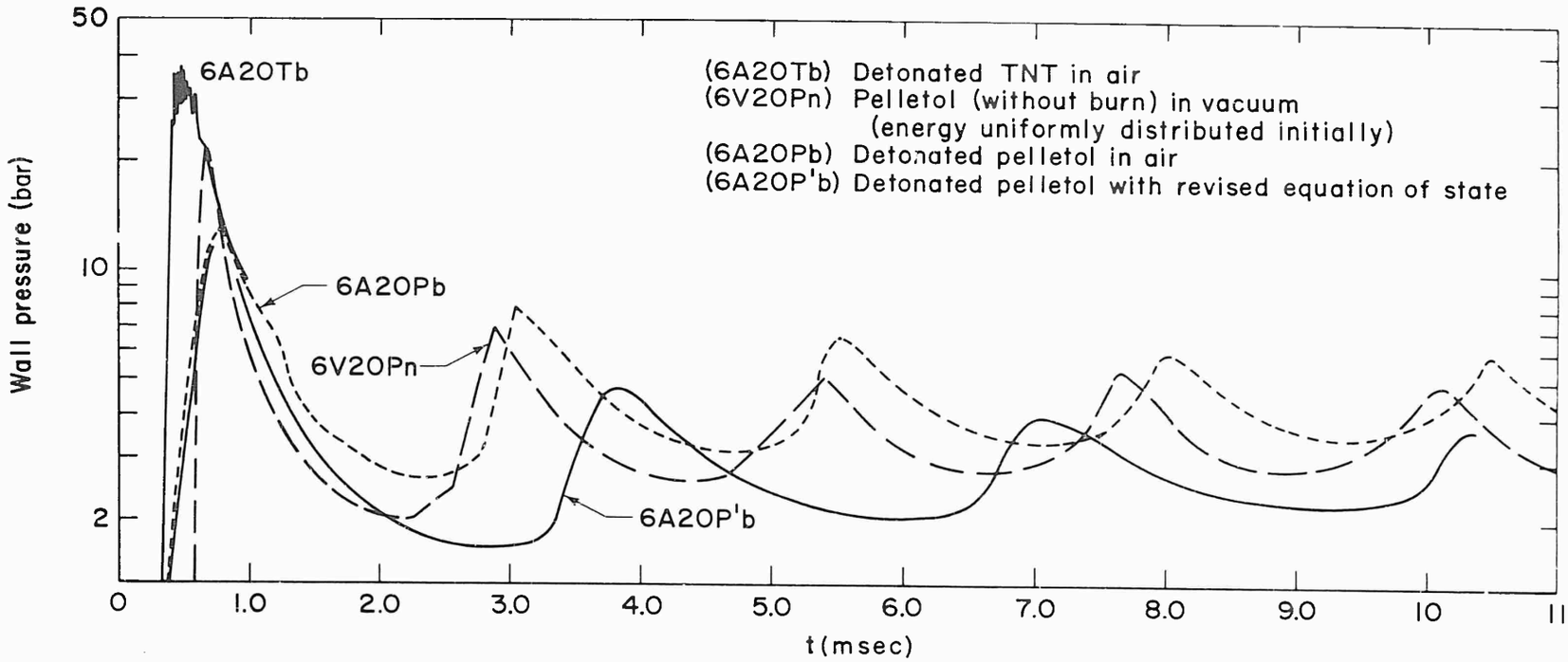

Fig. 1 - Comparison of cavity wall pressures versus time from four calculations for 9-kg charges in a 1.83-m radius cavity.

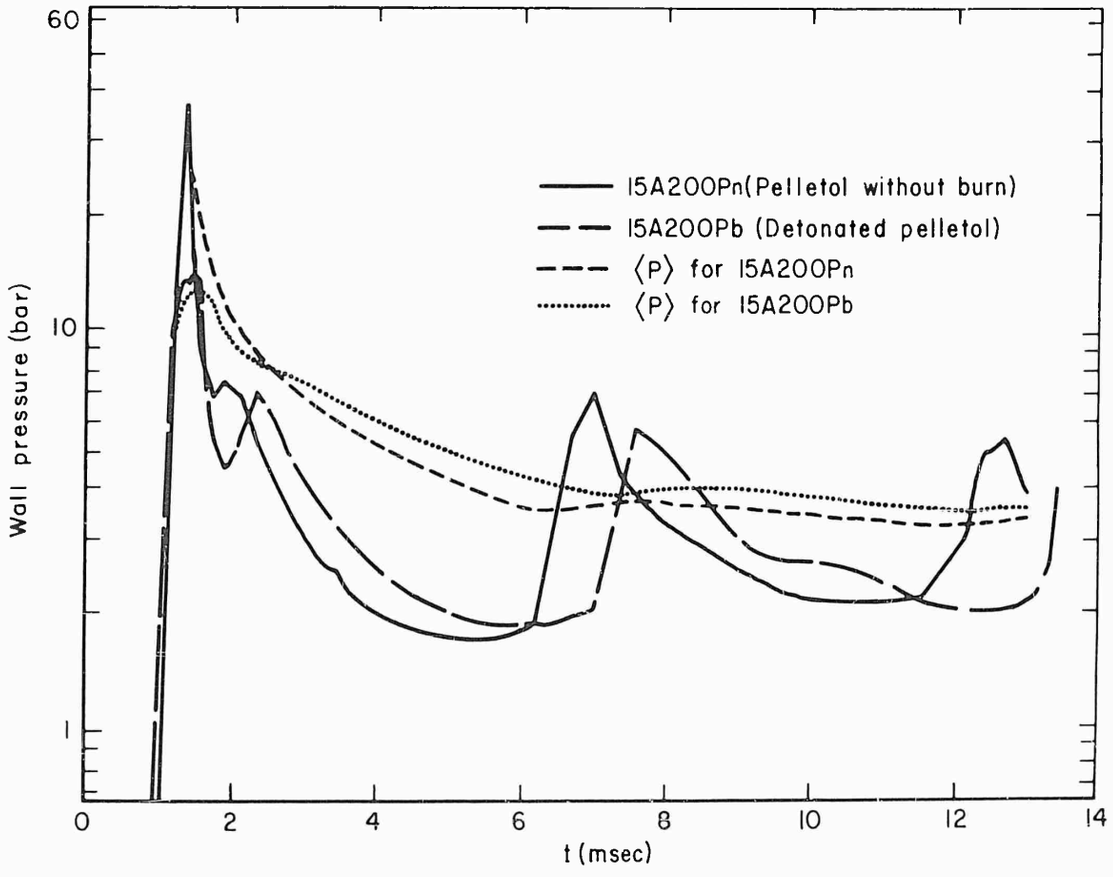

Fig. 2 - Comparison of wall pressures versus time from calculations for 90-kg charges of Pelletol in a 4.57-m radius cavity.

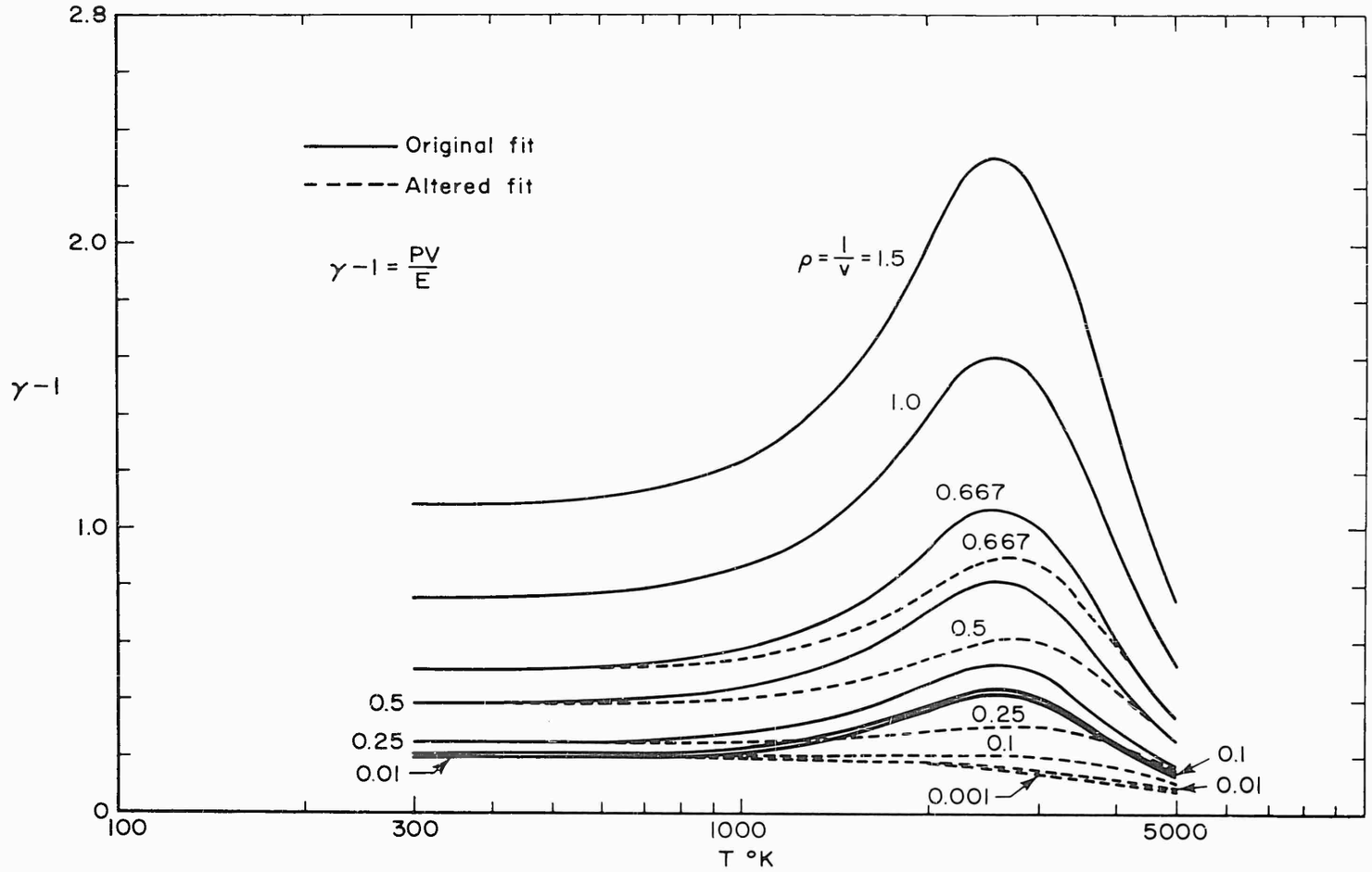

Fig. 3 - Equation of state of Pelletol based on Jones and Miller adiabatic data.

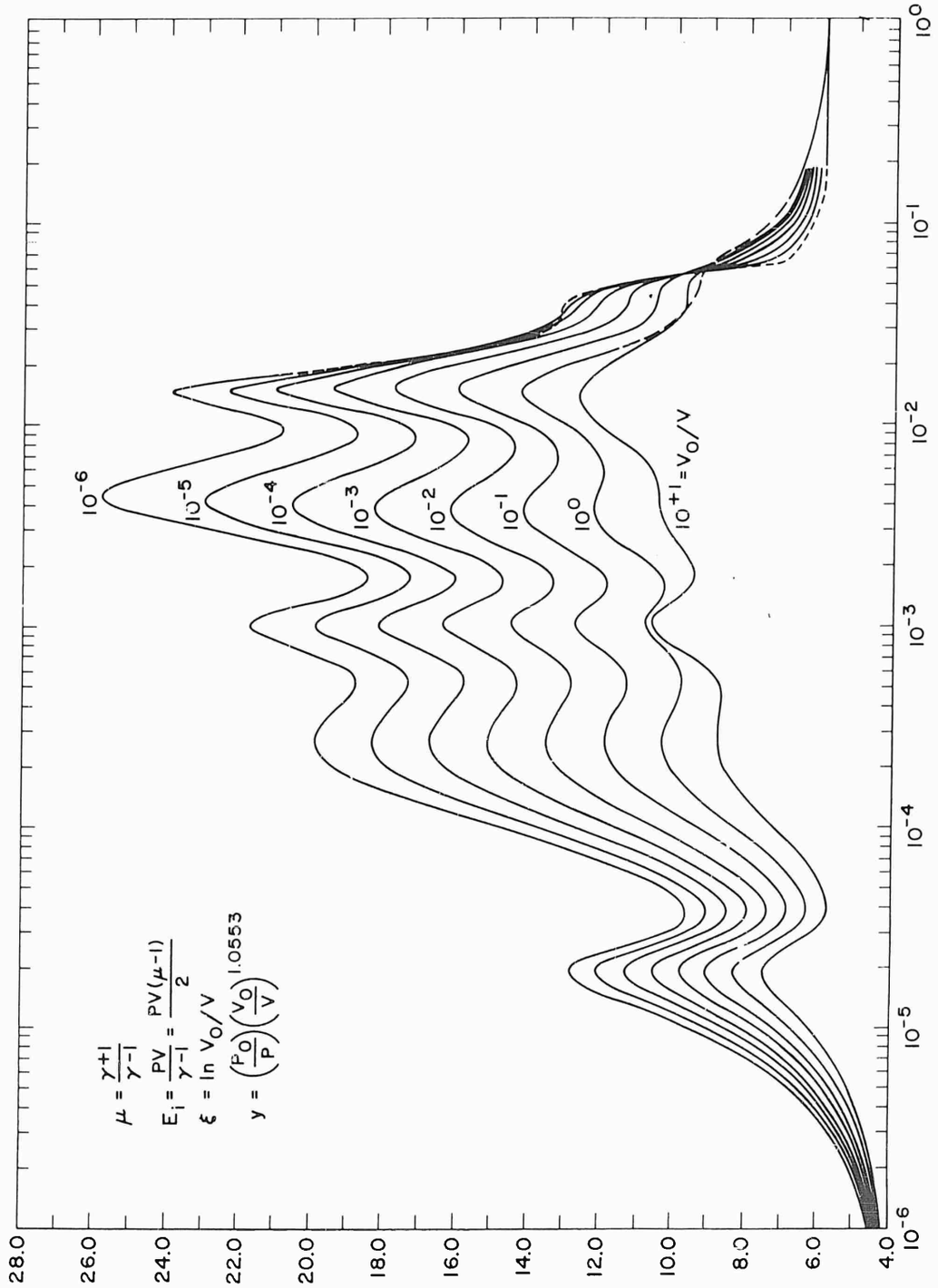

Fig. 4 - Graph of equation 8.

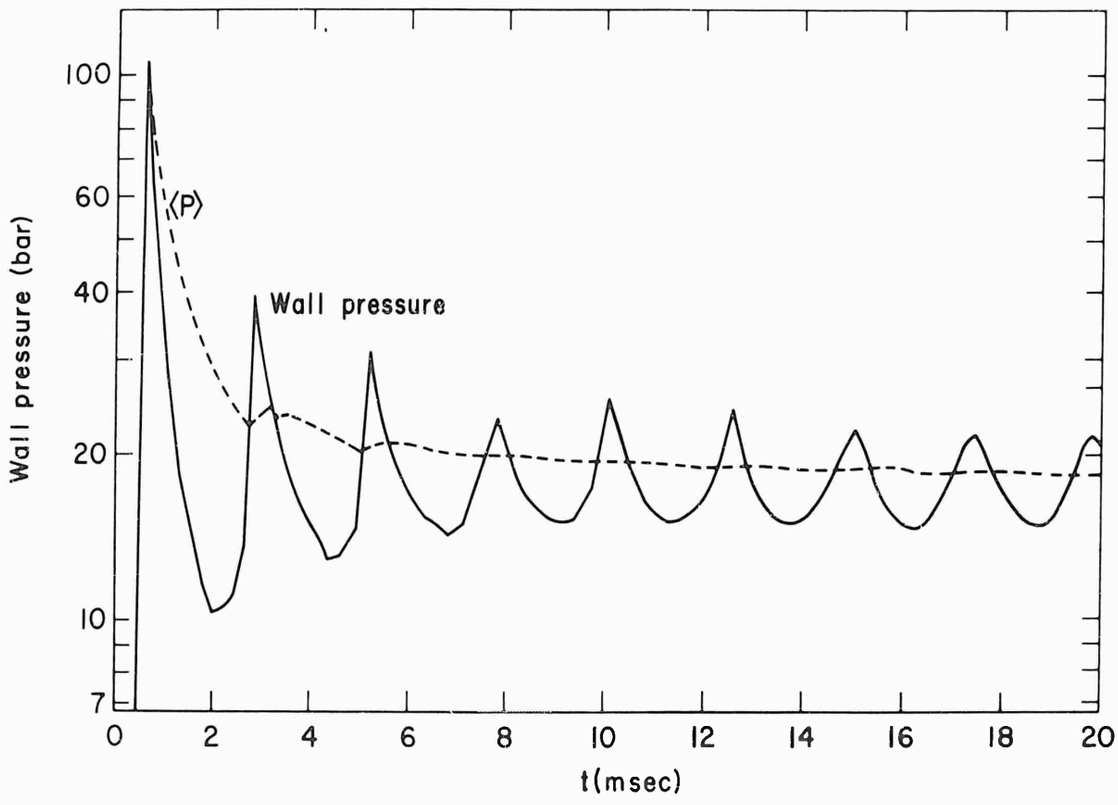

Fig. 5 - Wall pressure and wall pressure average versus time for a 45-kg charge of Pelletol detonated in a 1.83-m radius evacuated cavity.

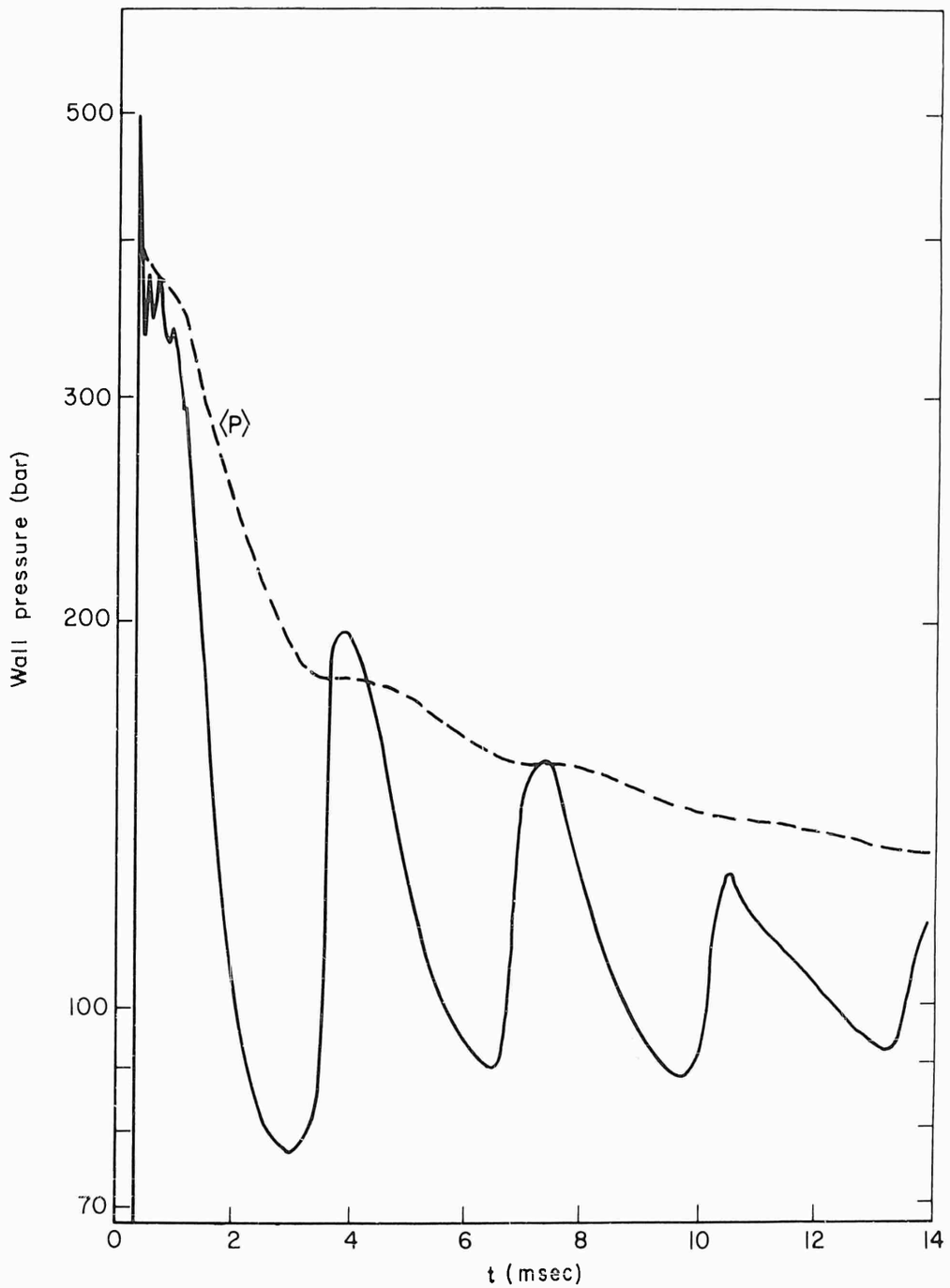

Fig. 6 - Wall pressure and wall pressure average versus time for a 450-kg charge of Pelletol detonated in a 1.83-m radius evacuated cavity.

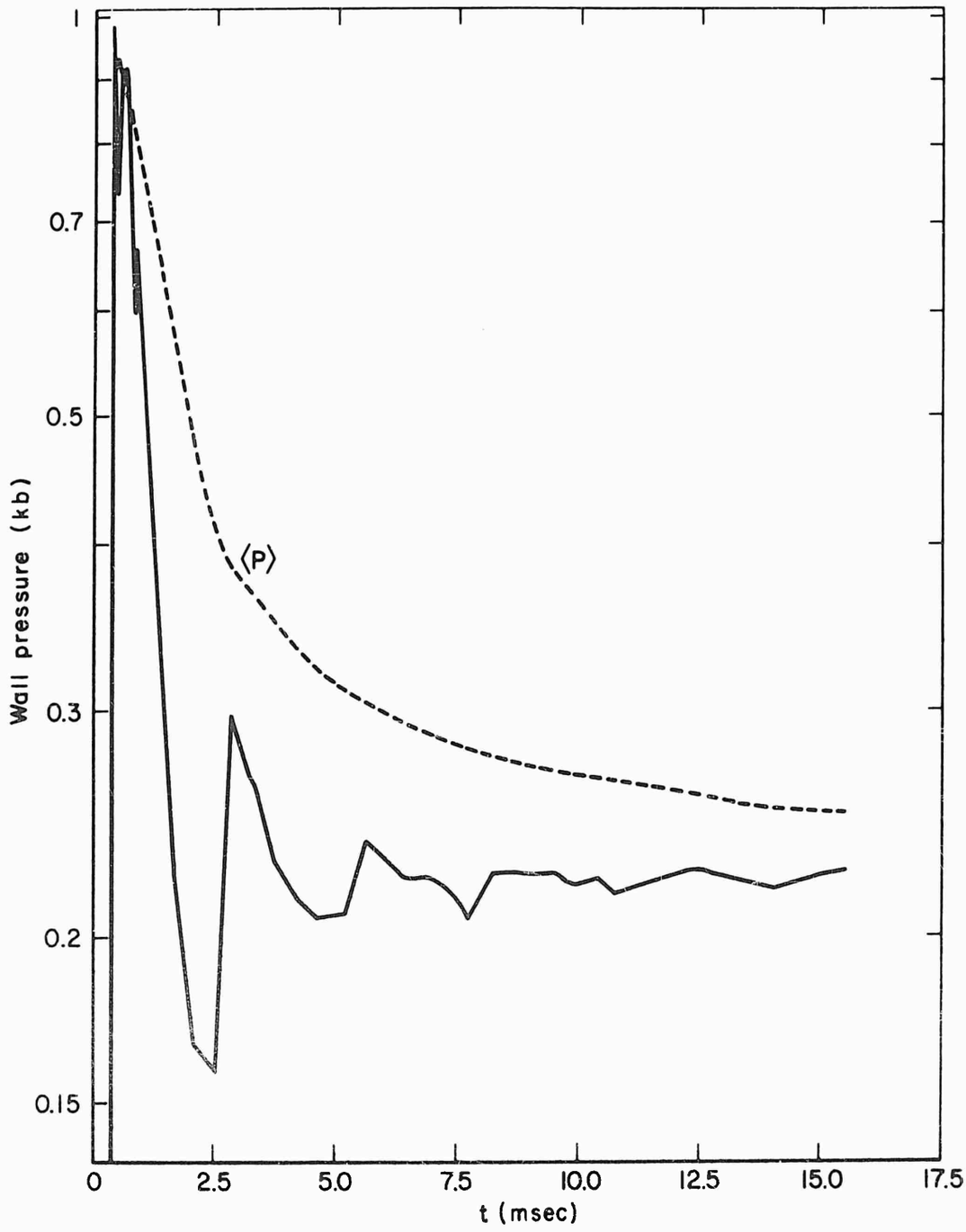

Fig. 7 - Wall pressure and wall pressure average versus time for a 900-kg charge of Pelletol detonated in a 1.83-m radius evacuated cavity.

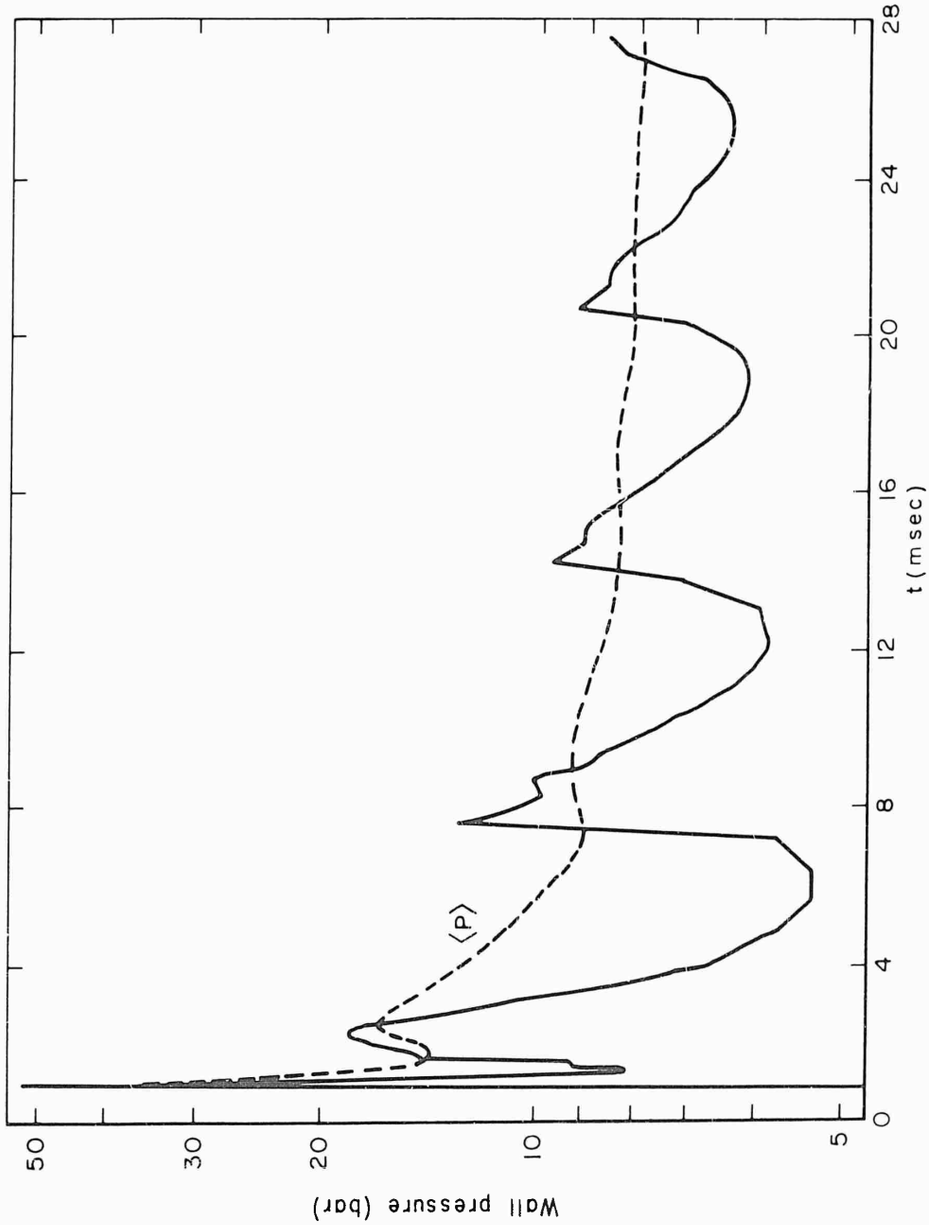

Fig. 8 - Wall pressure and wall pressure average versus time for a 230-kg charge of Pelletol detonated in a 4.57-m radius evacuated cavity.

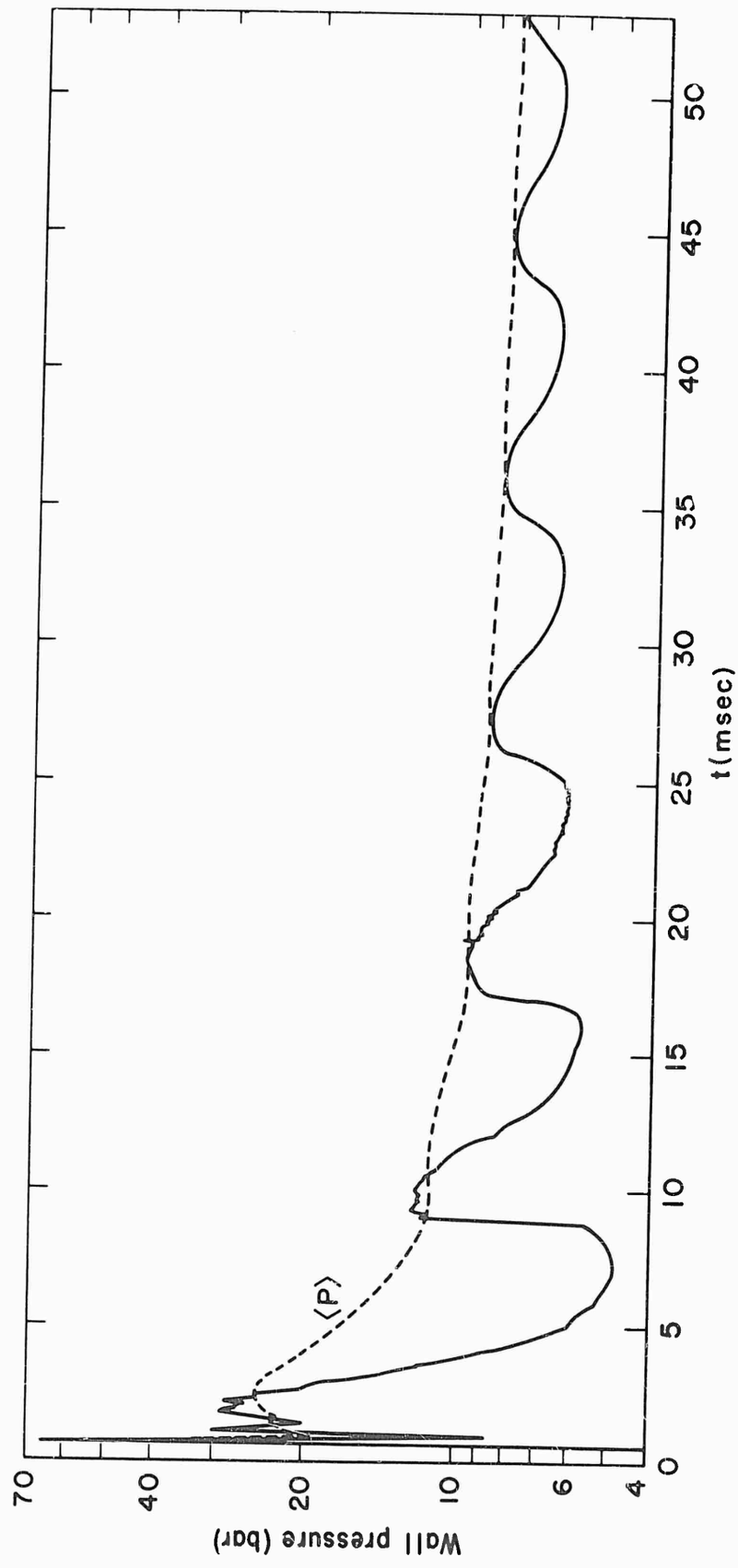

Fig. 9 - Wall pressure and wall pressure average versus time for a 450-kg charge of Pelletol detonated in a 4.57-m radius evacuated cavity.

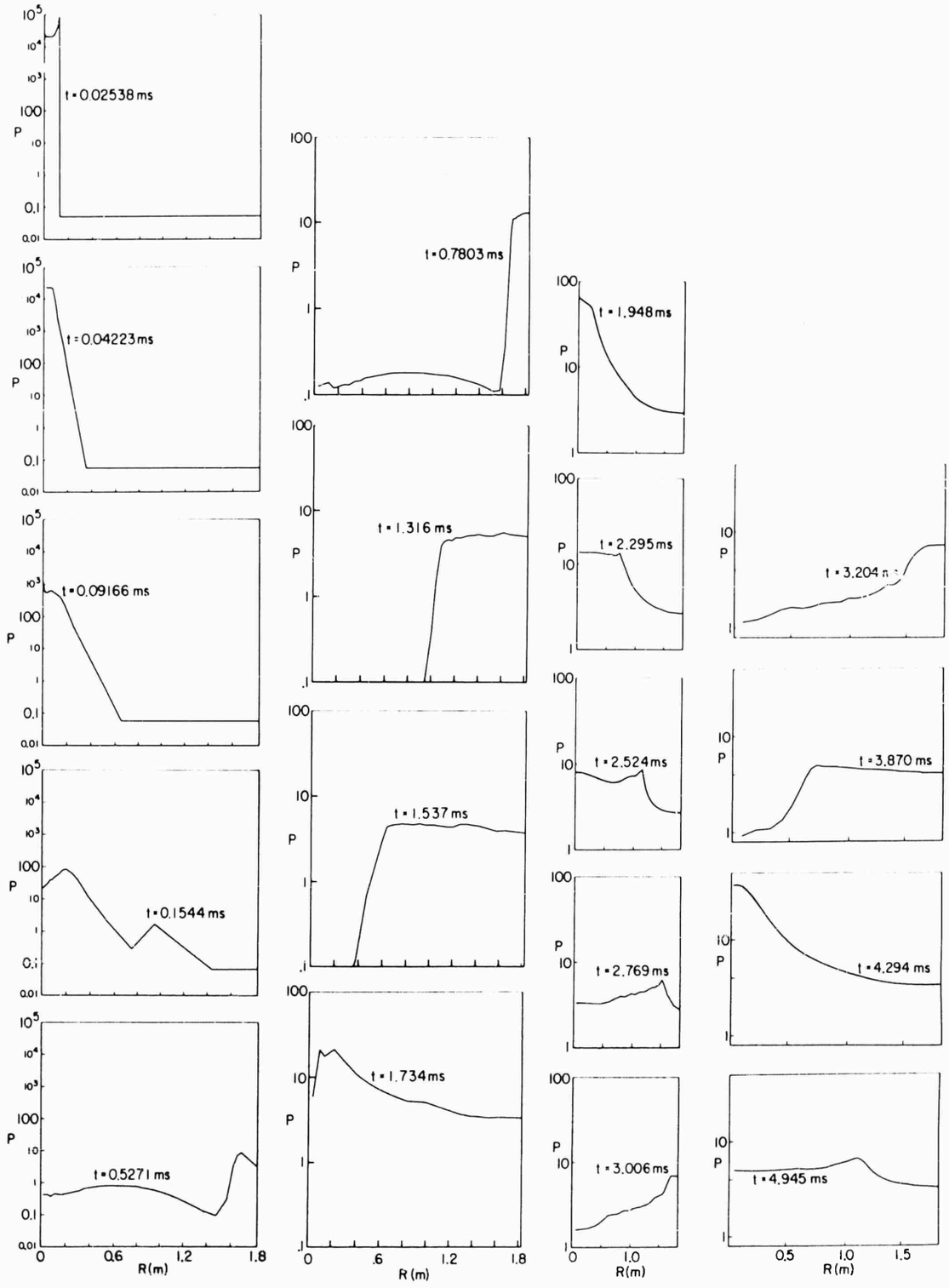

Fig. 10 - Pressure (bars) versus radius at indicated time during explosion of a 9-kg charge of Pelletol detonated in a 1.83-m radius cavity.

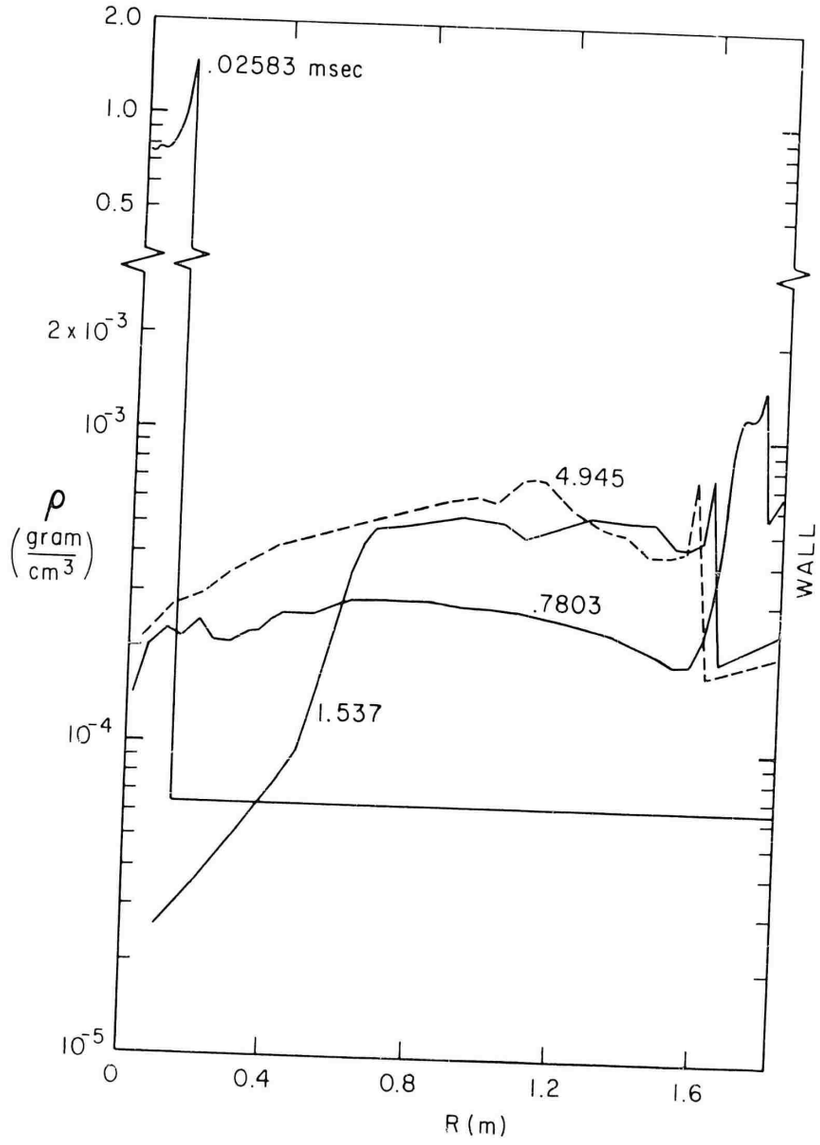

Fig. 11 - Density versus radius at indicated times during the explosion of a 9-kg charge of Pelletol detonated in a 1.83-m radius cavity.

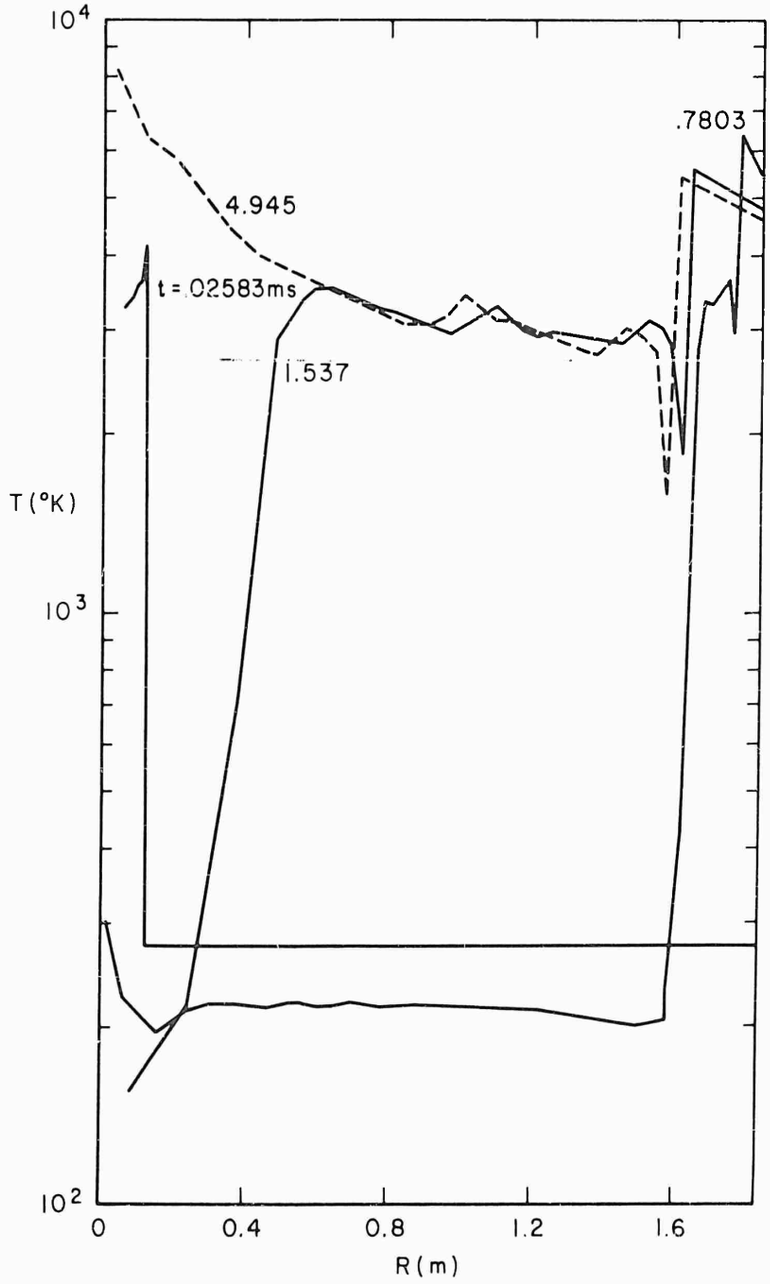

Fig. 12 - Temperature versus radius at indicated times during the explosion of a 9-kg charge of Pelletol detonated in a 1.83-m radius cavity.

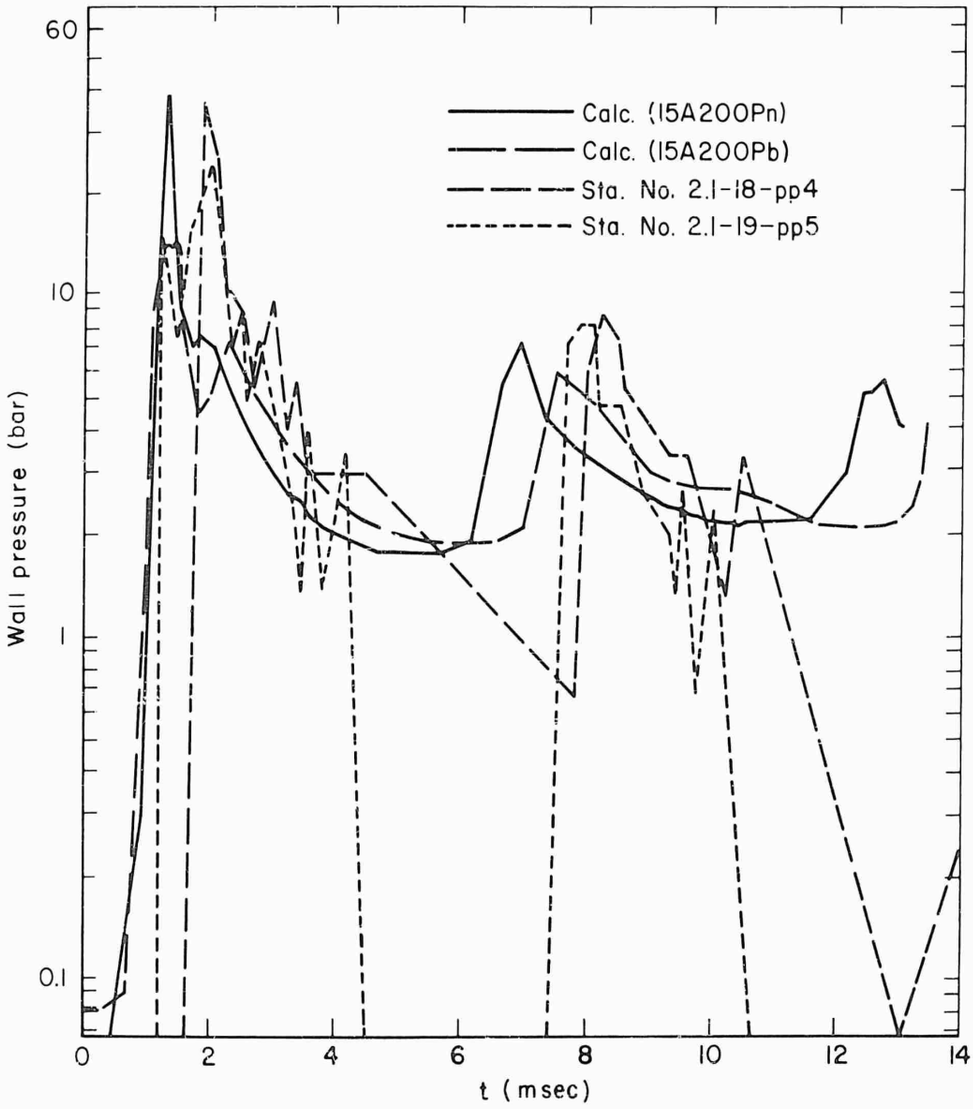

Fig. 13 - Comparison of wall pressure data with calculation for 90-kg of Pelletol in a 4.57-m radius cavity.

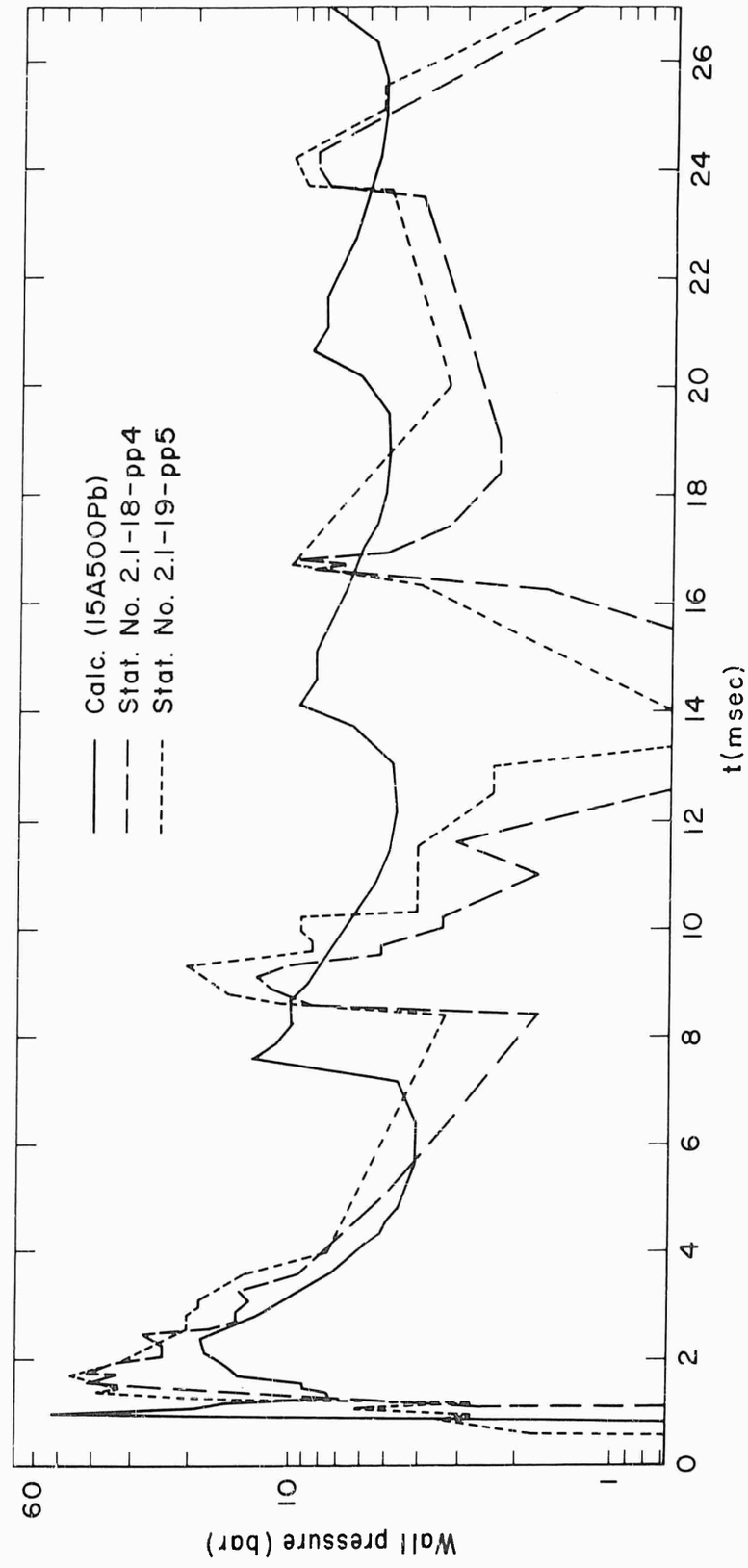

Fig. 14 - Comparison of wall pressure data with calculation for 230-kg of Pelletol in a 4.57-m radius cavity.

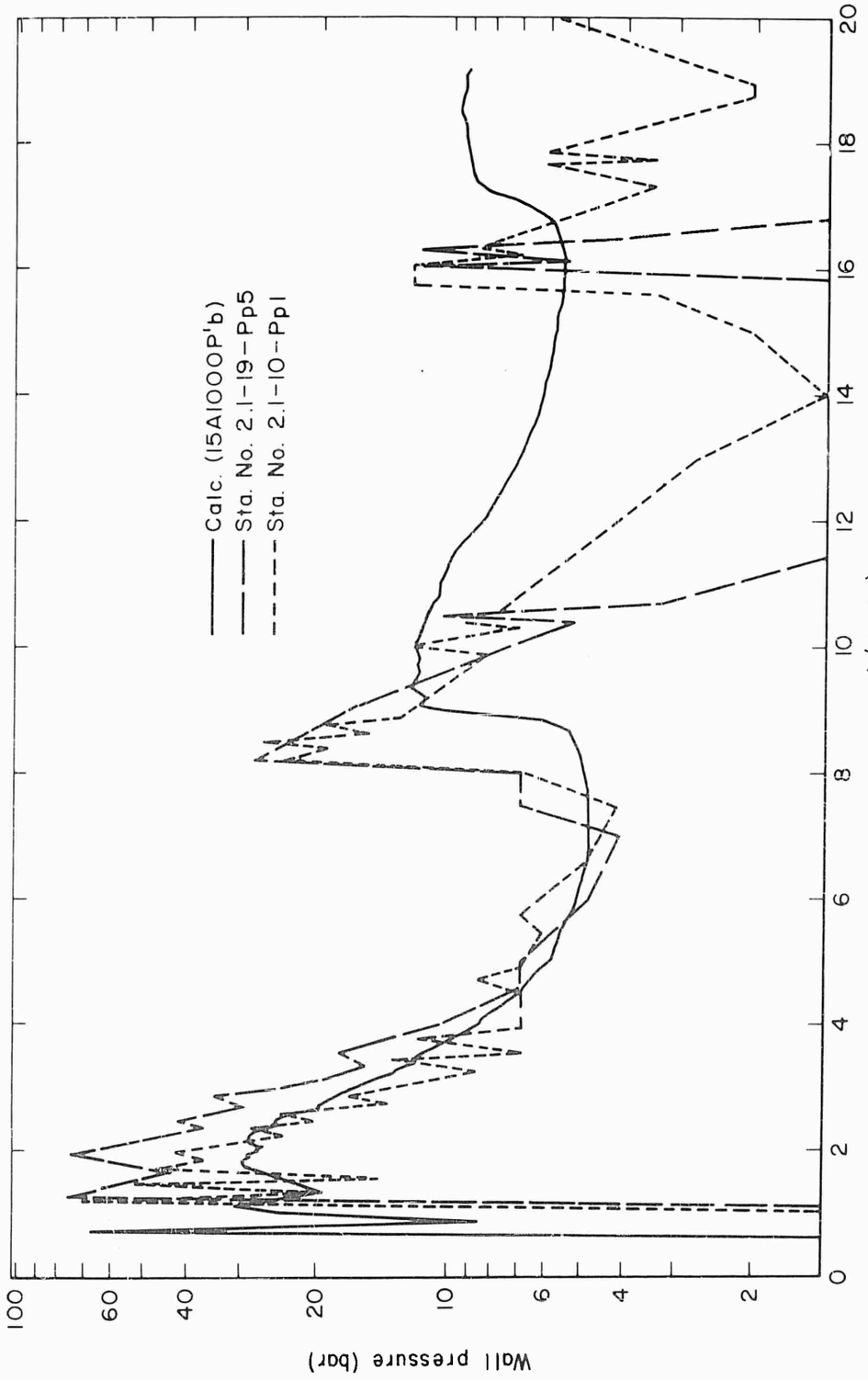

Fig. 15 - Comparison of wall pressure data with calculation for 450-kg of Pelletol in a 4.57-m radius cavity.

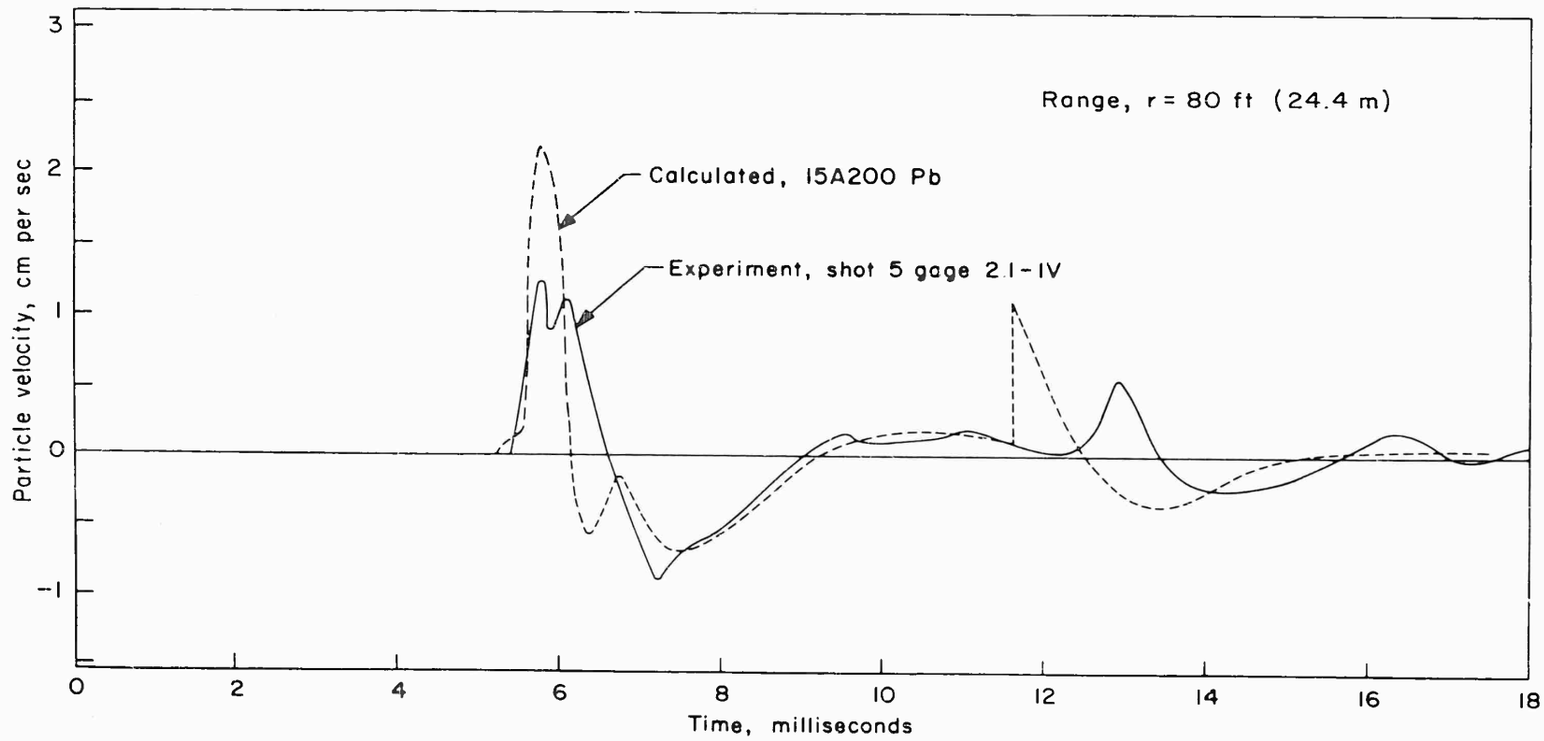

Fig. 16 - Measured and calculated radial particle velocities in salt for 90-kg of Pelletol charge in a 4.57-m radius cavity.

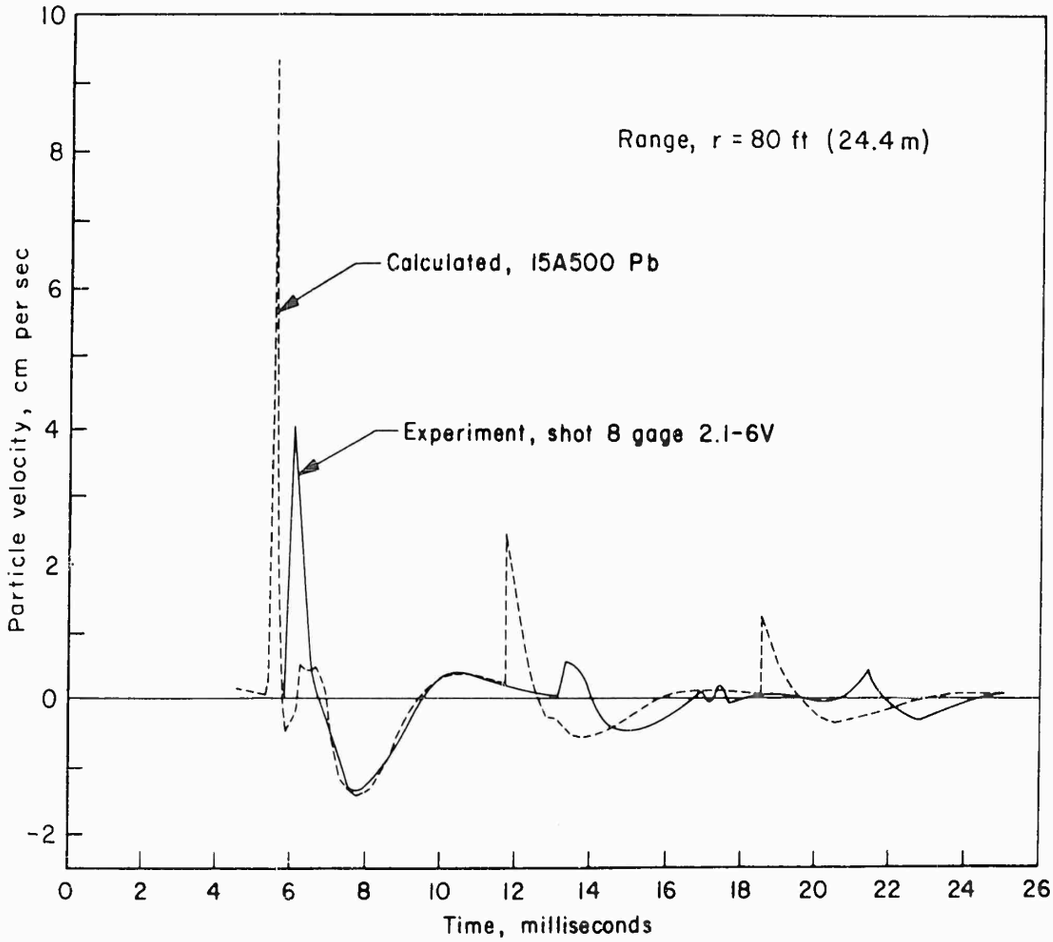

Fig. 17 - Measured and calculated radial particle velocities in salt for a 230-kg Pelletol charge in a 4.57-m radius cavity.

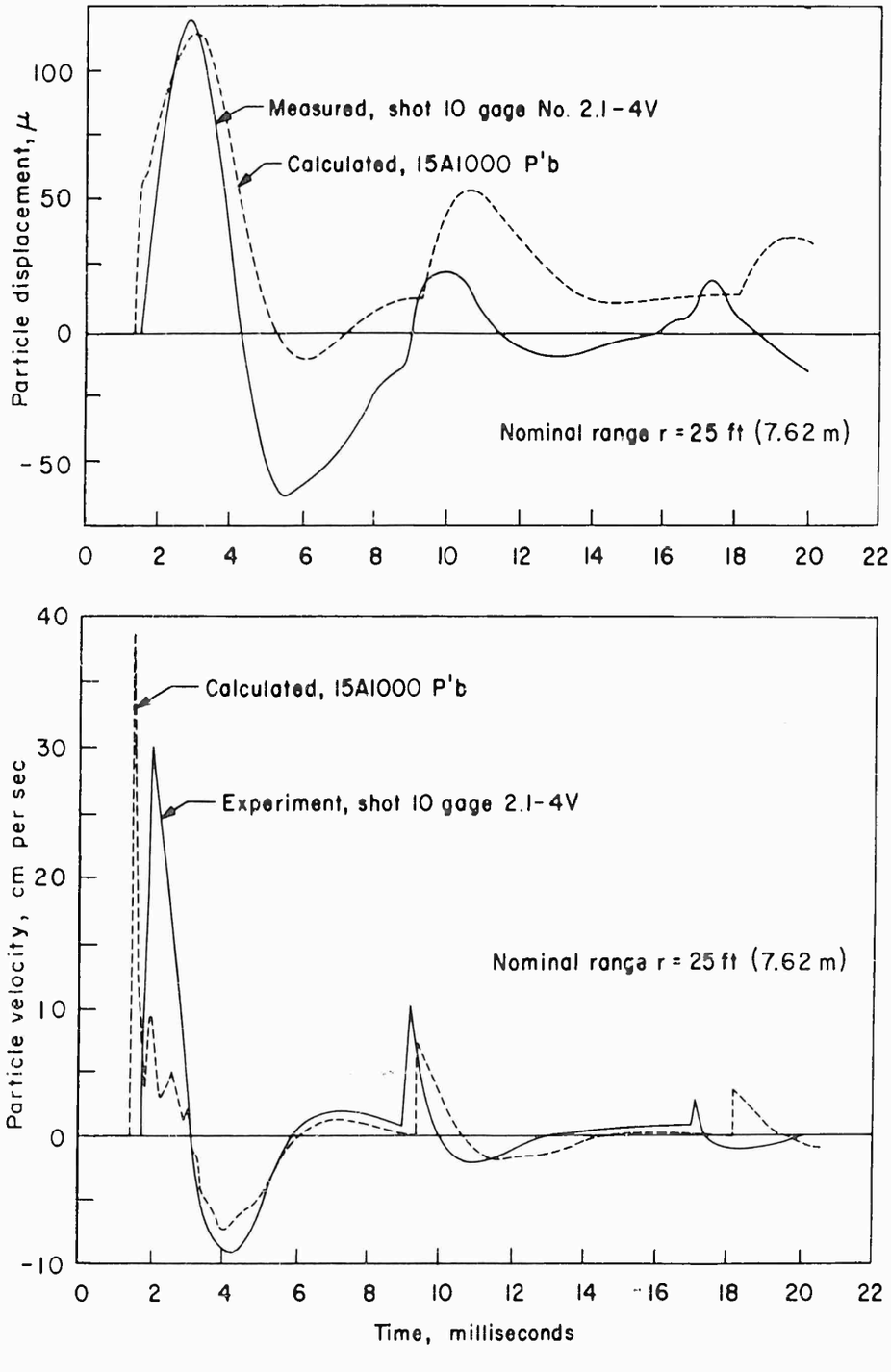

Fig. 18 - Particle displacements and velocities in salt at twenty-five foot (7.62-m) range for 450-kg Pelletol charges in a 4.57-m radius cavity.

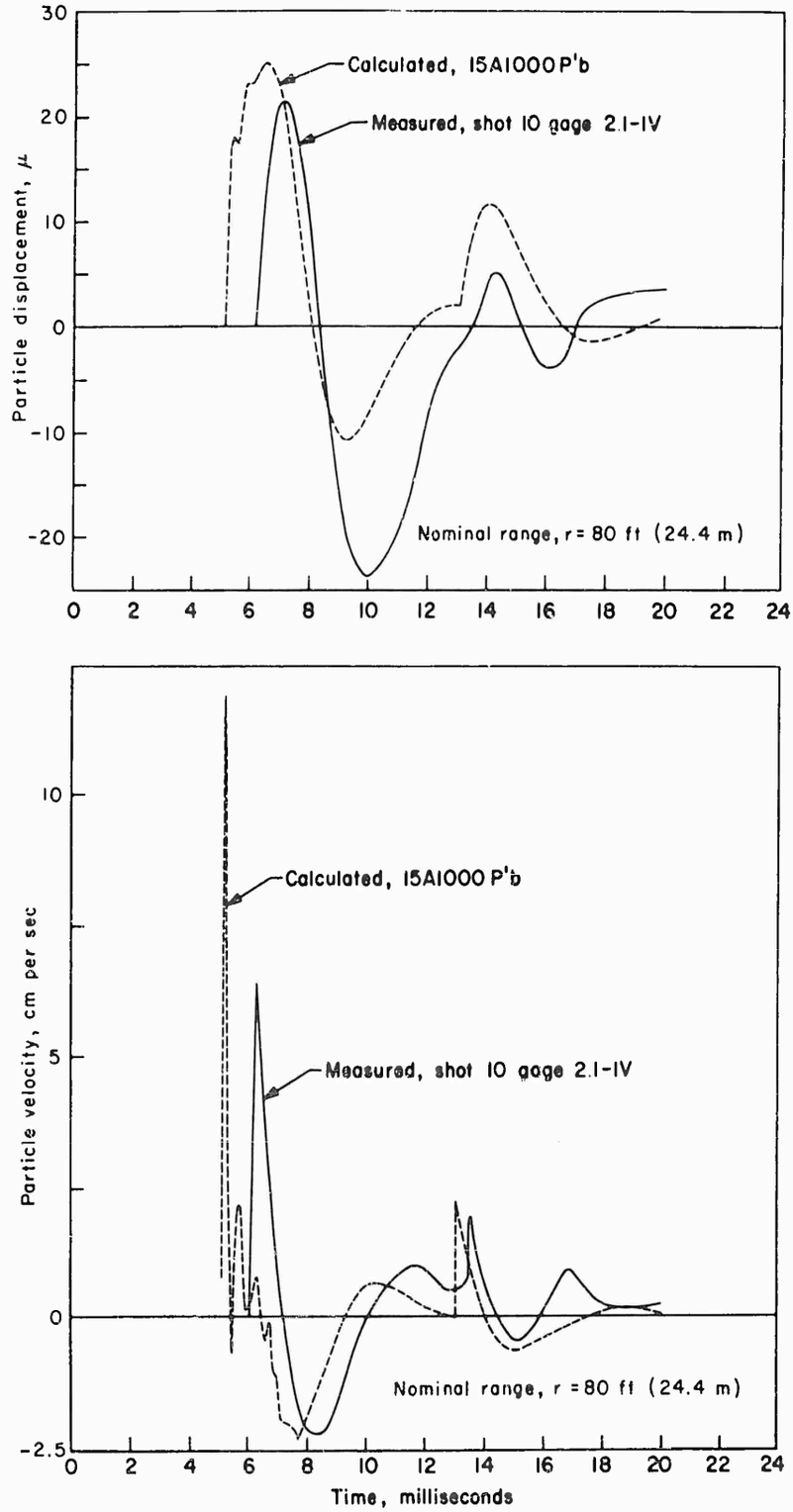

Fig. 19 - Particle displacements and velocities in salt at an eighty foot (24.4-m) range for 450-kg Pelletol charges in a 4.57-m radius cavity.

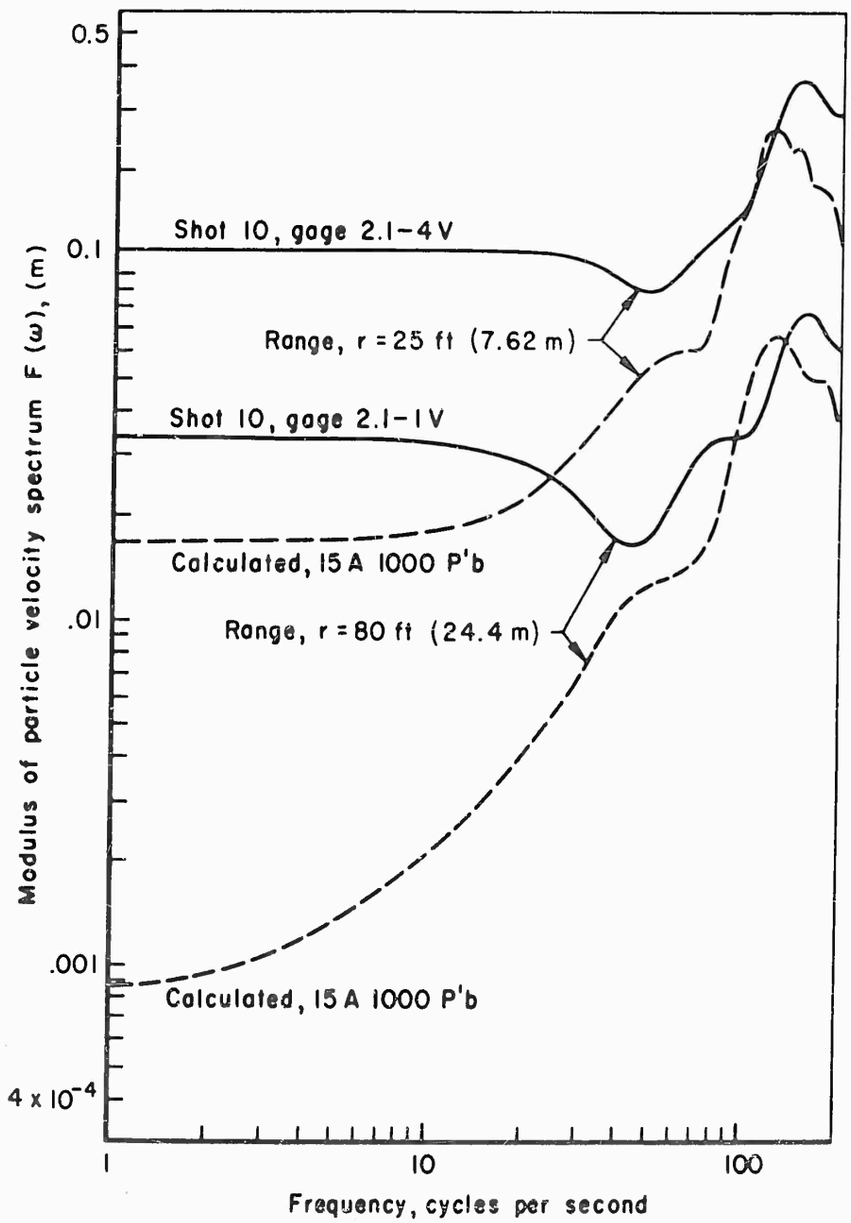

Fig. 20 - Comparison of spectrums derived from experimental and theoretical particle velocities.

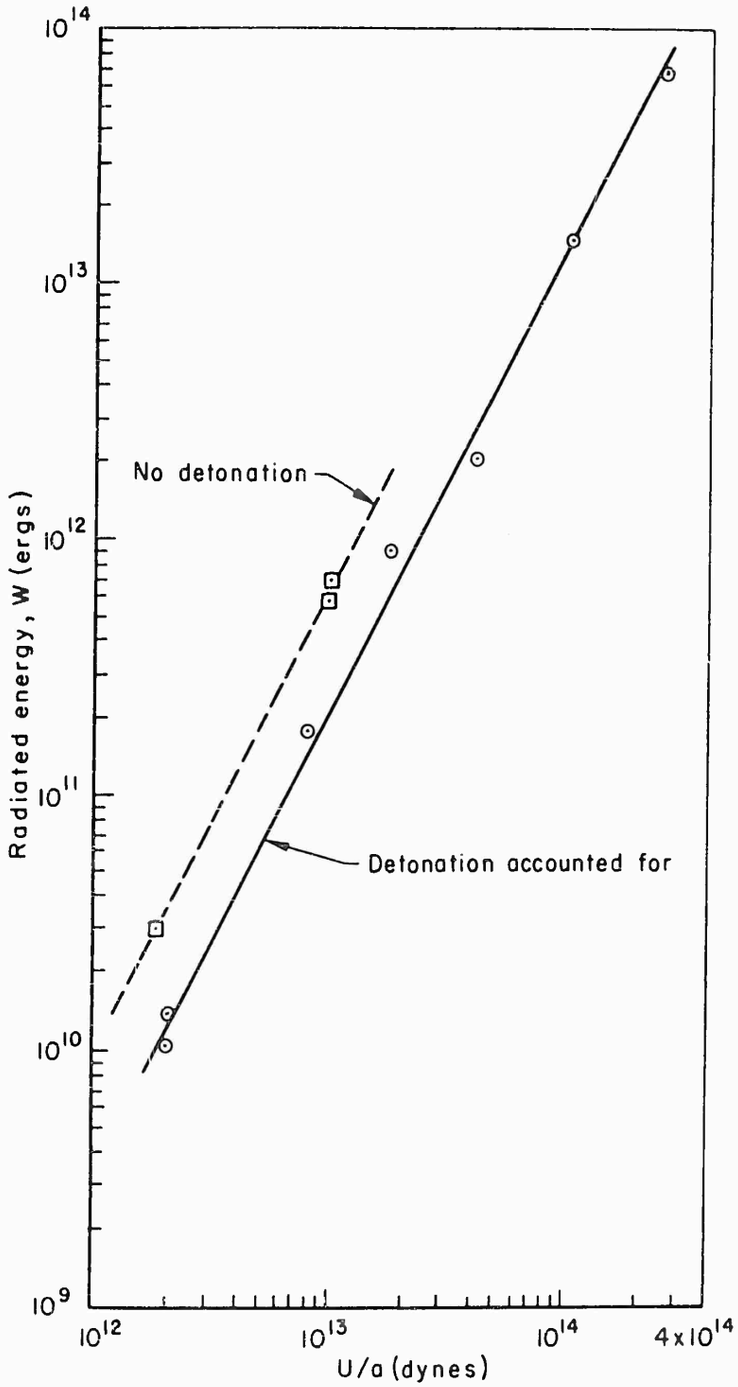

Fig. 21 - Power-law correlation between radiated and explosive energies.

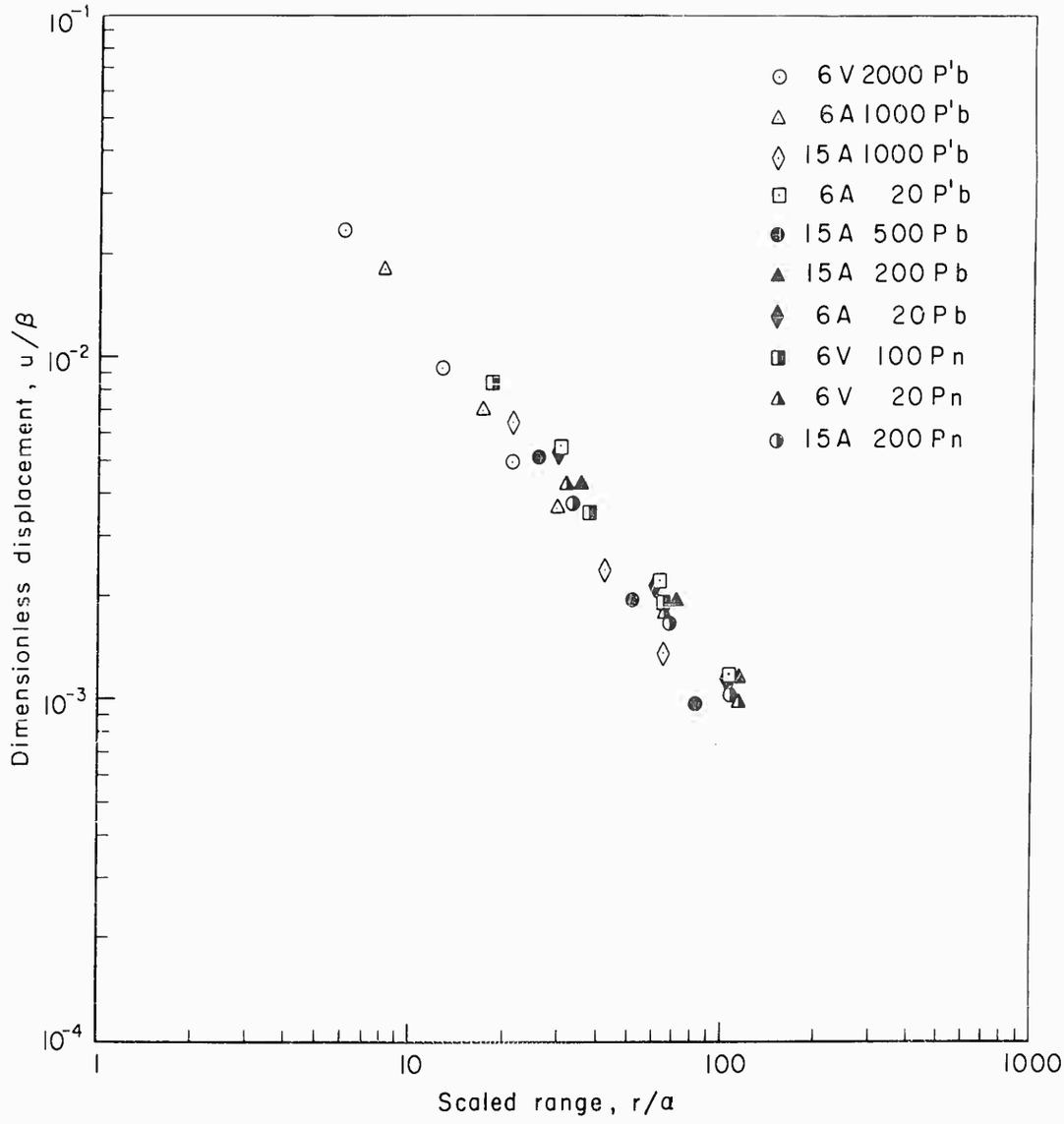

Fig. 22 - Theoretical peak particle displacements versus scaled range.

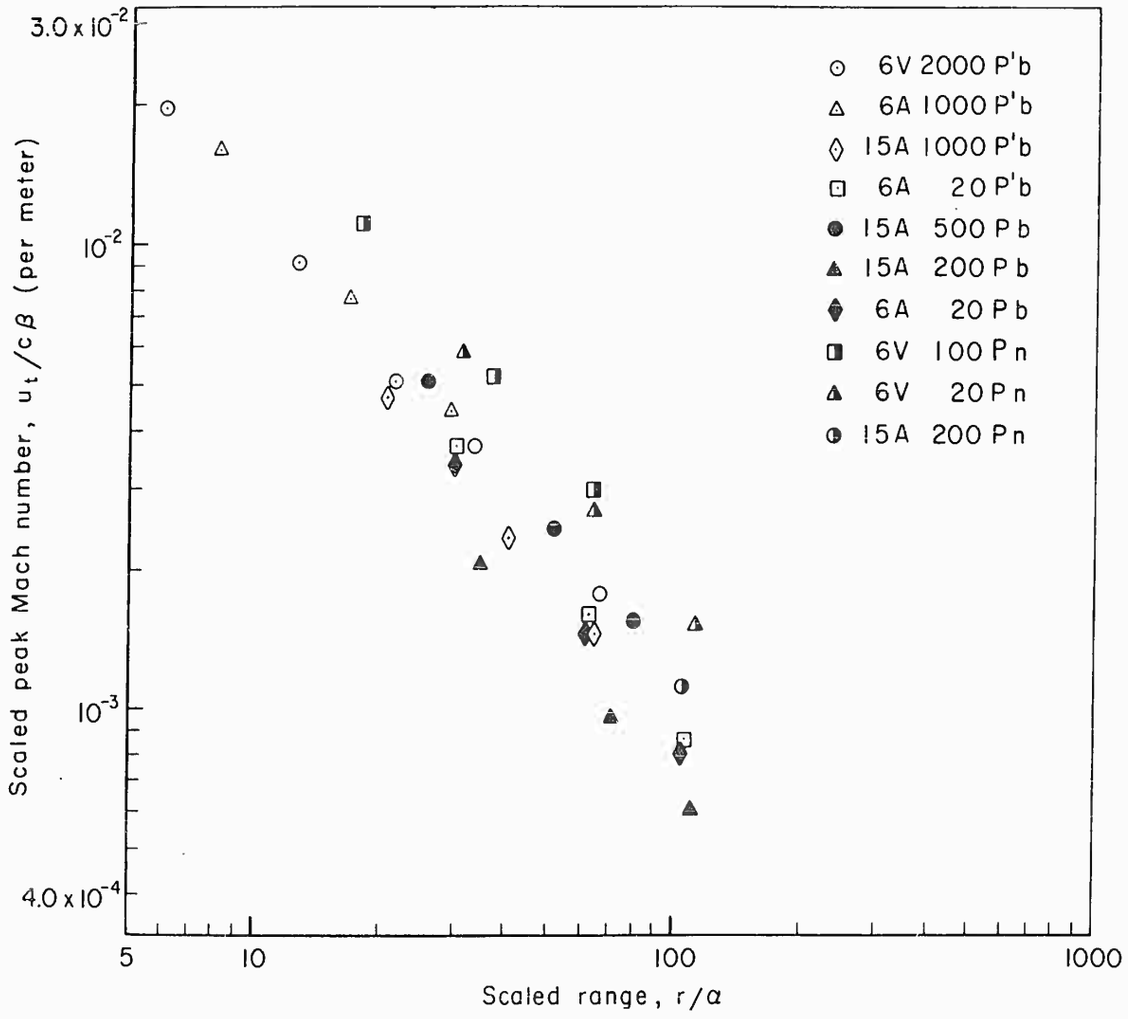

Fig. 23 - Theoretical peak particle velocities versus scaled range.

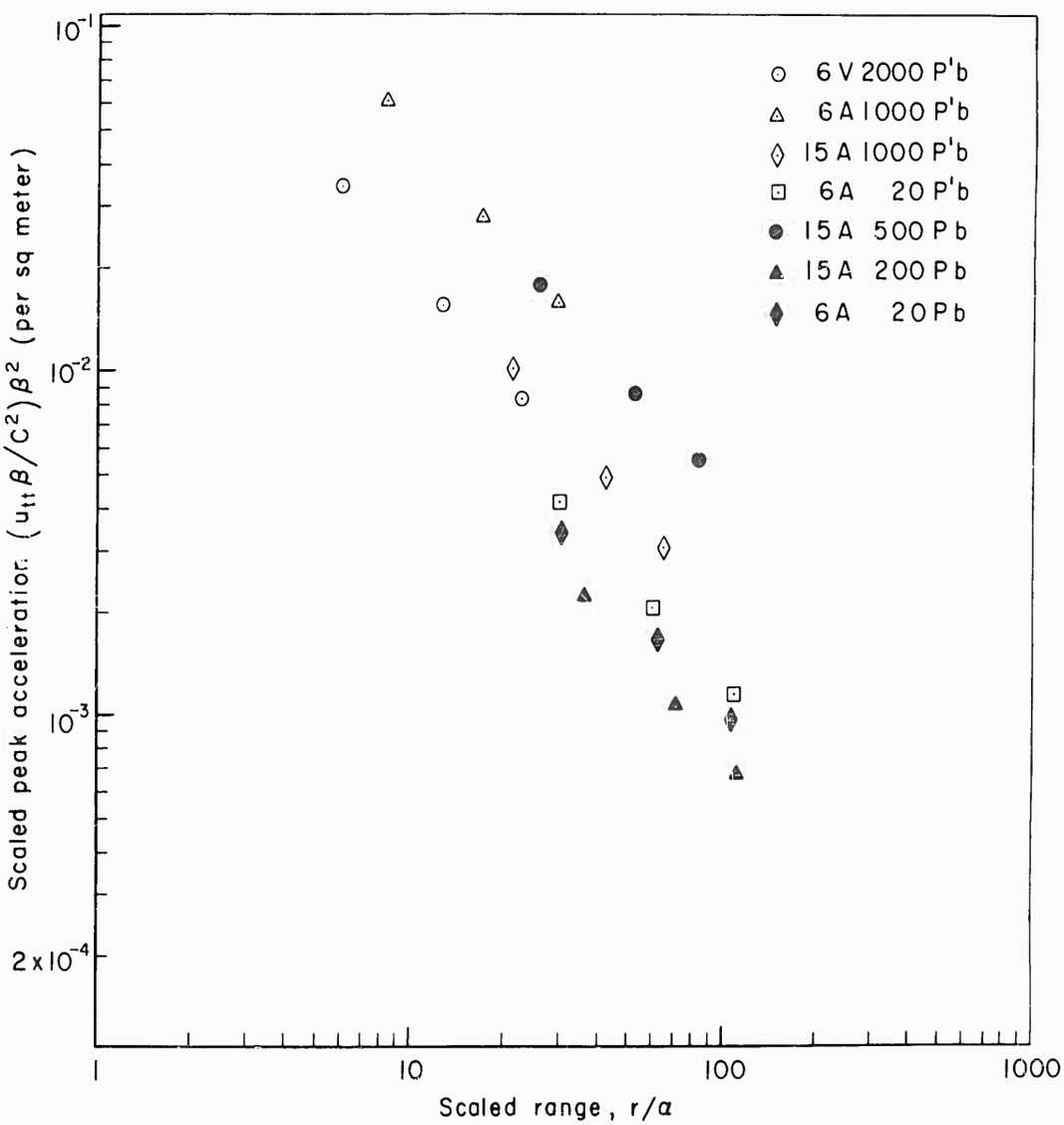

Fig. 24 - Theoretical peak particle accelerations versus scaled range.

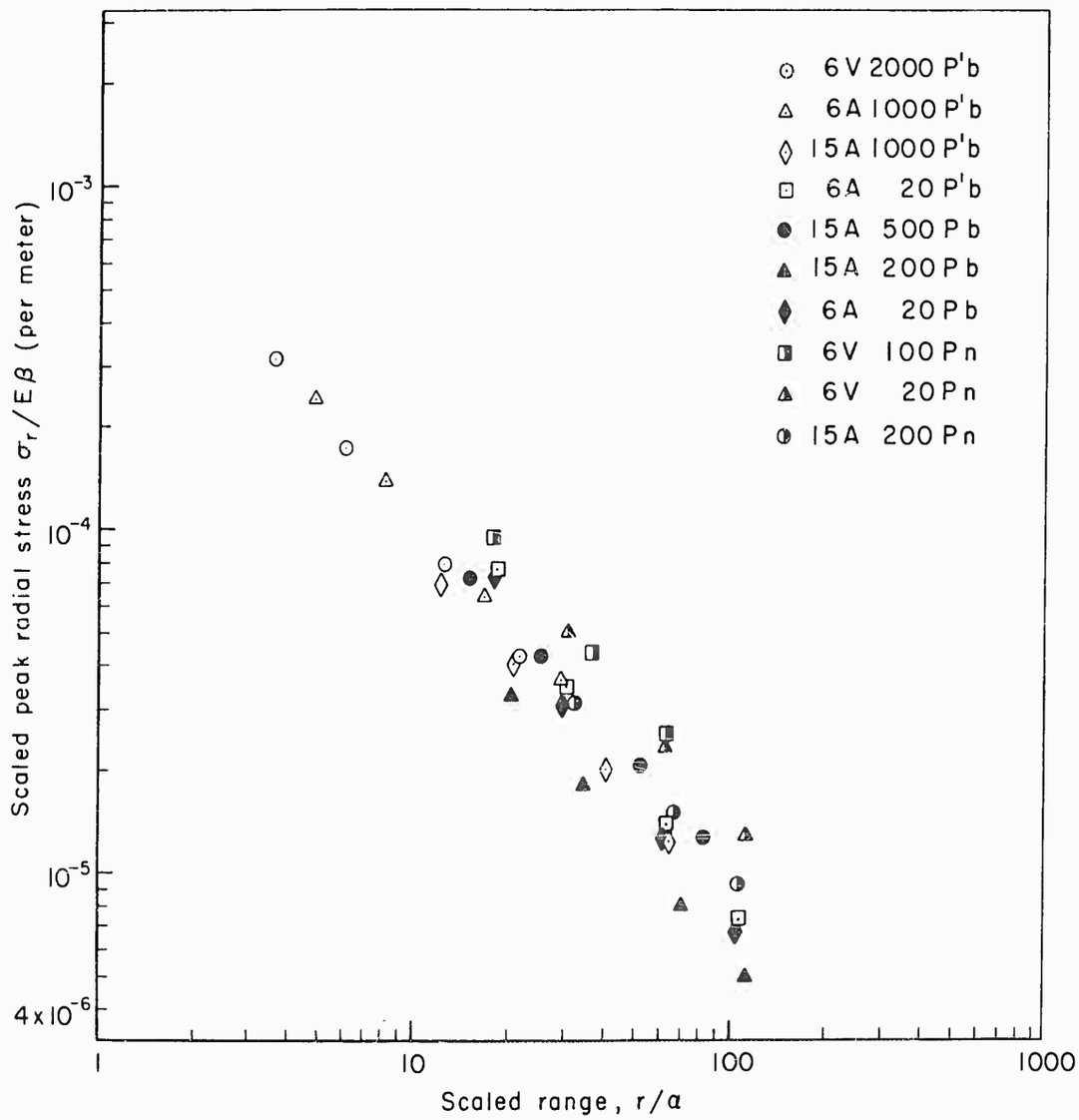

Fig. 25 - Theoretical peak radial stresses versus scaled range.

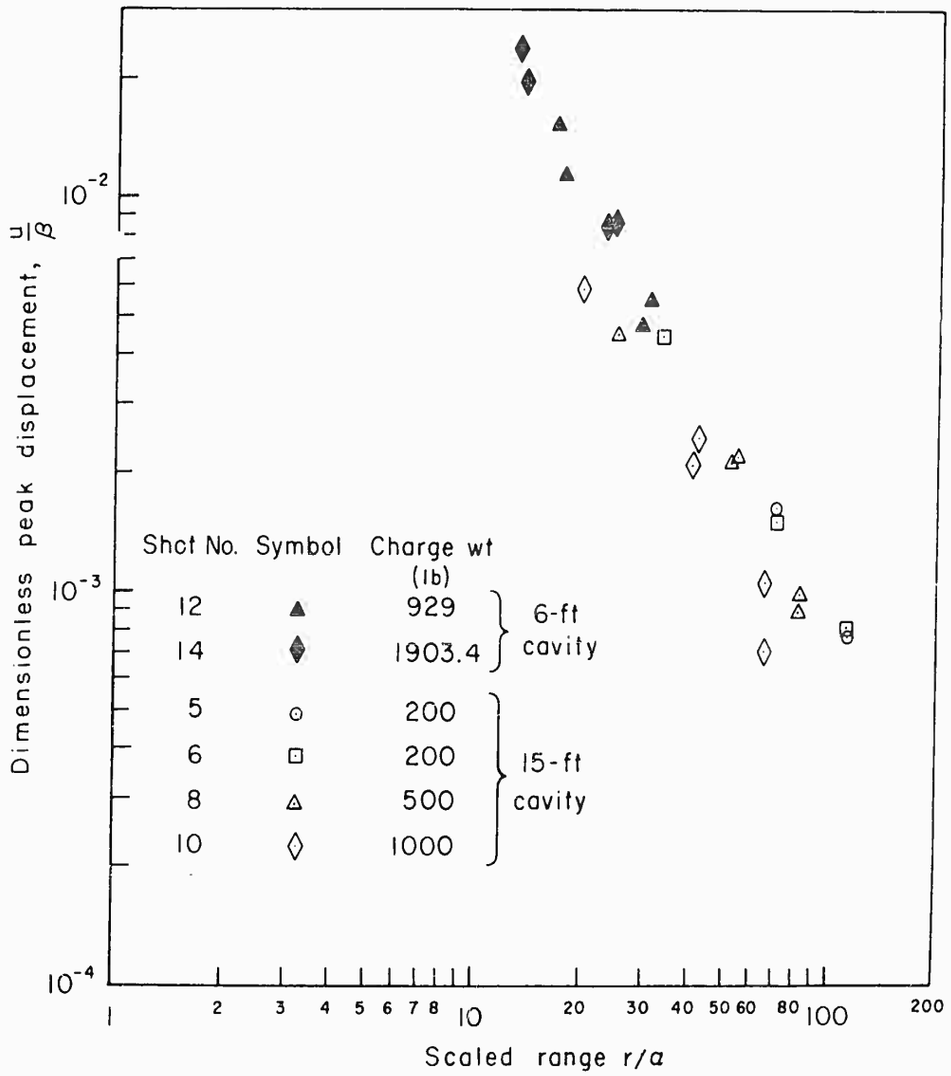

Fig. 26 - Correlation for the experimental data of peak particle displacement in the salt at various distances from the center of the cavities.

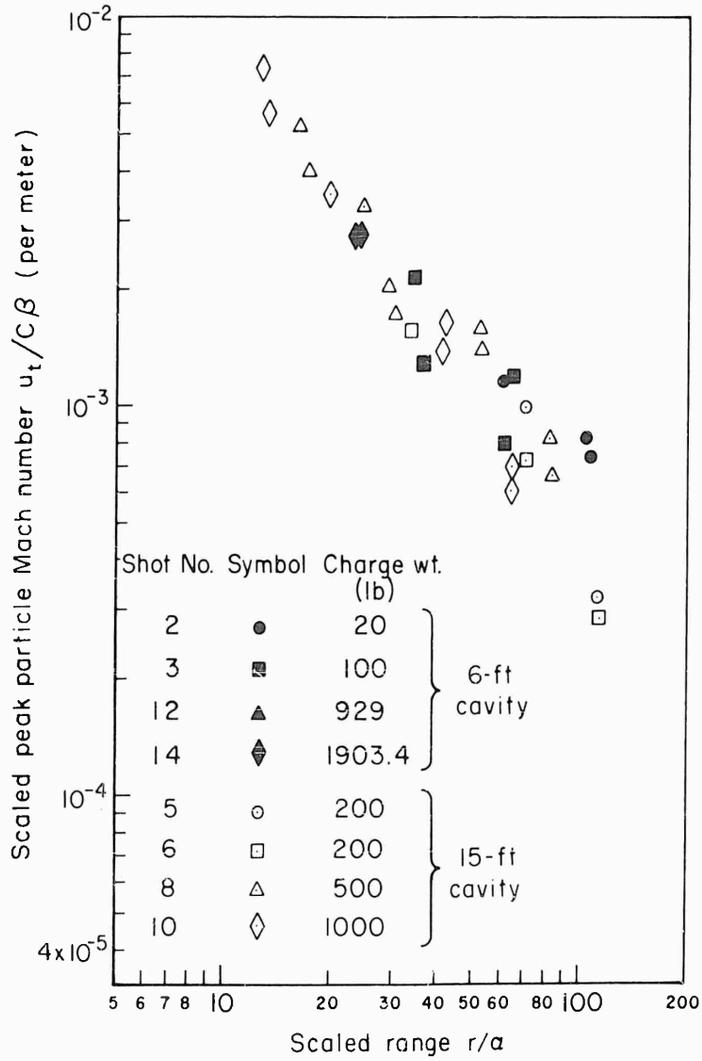

Fig. 27 - Correlation for the experimental data of peak particle velocity in the salt at various distances from the center of the cavities.

REFERENCES

Adams, W. M., and D. C. Allen, Seismic decoupling for explosives in spherical underground cavities, Geophysics, 26 (6), 772, 1961.

Brode, H. L., Cavity explosion calculations for the Cowboy program, The RAND Corporation, Res. Memo. RM-2624-AEC, August 5, 1960.

Brode, H. L., Numerical solutions of spherical blast waves, J. Appl. Phys. 26, 766, 1955.

Brode, H. L., Blast wave from a spherical charge, Phys. Fluids, 2, 217, 1959.

Eringen, A. C., Elasto-dynamic problem concerning the spherical cavity, Quart. J. Mech. Appl. Math., 10, Part 3, 257, August 1957.

Gilmore, F. R., Equilibrium composition and thermodynamic properties of air to 24,000°K, The RAND Corporation, Res. Memo. RM-1543, August 24, 1955.

Herbst, R. F., G. C. Werth, and D. L. Springer, Use of large cavities to reduce seismic waves from underground explosions, J. Geophys. Res., 66 (3), 959-978, 1961.

Hilsenrath, J., and C. W. Beckett, Thermodynamic properties of argon-free air, Natl. Bur. Standards, Rept. 3991, April 1955.

Hopkins, H. G., Dynamic expansion of spherical cavities in metals, Chapter III of Progress in Solid Mechanics, (Sneddon and Hill, Editors), North-Holland Publishing Co., Amsterdam, p. 83, 1960.

Jones, H. and A. R. Miller, The detonation of solid explosives: the equilibrium conditions in the detonation wave-front and the adiabatic expansion of the products of detonation, Proc. Roy. Soc. London, A194, 480, 1948.

Latter, A. L., R. E. LeLevier, E. A. Martinelli, and W. G. McMillan, A method of concealing underground nuclear explosions, J. Geophys. Res., 66, 943-946, 1961.

Latter, A. L., E. A. Martinelli, and E. Teller, A seismic scaling law for underground explosions, Phys. Fluids, 2, 280-282, 1959.

Murphey, B. F., Particle motions near explosions in halite, J. Geophys. Res., 66 (3), 947, 1961.

Nicholls, H. R., V. Hooker, and W. I. Duvall, Dynamic rock mechanics investigations project Cowboy, U. S. Bureau of Mines Applied Physics Research Lab., College Park, Maryland, Rept. APRL 38-3.2, Sept. 1, 1960.

Parkin, B. R., A review of similitude theory in ground shock problems, The RAND Corporation, Res. Memo RM-2173, April 22, 1958.

Parkin, B. R., Elastic wave calculations for the Cowboy program, The RAND Corporation, Res. Memo RM-3105-AEC, May 1962.

Thomas, T. Y., Plastic Flow and Fracture in Solids, Academic Press, New York, p. 16, 1961.

Von Neumann, J., and R. D. Richtmyer, A method for the numerical calculation of hydrodynamic shocks, J. Appl. Phys., 21, 232, 1950.